JGR Biogeosciences

RESEARCH ARTICLE
10.1029/2020JG006000

Investigating Thaw and Plant Productivity Constraints on Old Soil Carbon Respiration From Permafrost

Marguerite Mauritz[1], Elaine Pegoraro[2], Kiona Ogle[2,3], Christopher Ebert[2], and Edward A. G. Schuur[2]

[1]Univeristy of Texas, El Paso, TX, USA, [2]Center for Ecosystem Science and Society, Northern Arizona University, Flagstaff, AZ, USA, [3]School of Informatics, Computing, and Cyber Systems, Norther Arizona University, Flagstaff, AZ, USA

Key Points:

- Old soil respiration tripled from August to September and was highest from plots thawing at organic-to-mineral transition horizon
- Surface soil temperature best predicted seasonal increases in old soil respiration highlighting controls other than thaw depth
- Old soil contributions to ecosystem respiration were well constrained using a process-based isotope partitioning model

Supporting Information:

Supporting Information may be found in the online version of this article.

Correspondence to:

M. Mauritz,
memauritz@utep.edu

Citation:

Mauritz, M., Pegoraro, E., Ogle, K., Ebert, C., & Schuur, E. A. G. (2021). Investigating thaw and plant productivity constraints on old soil carbon respiration from permafrost. *Journal of Geophysical Research: Biogeosciences*, *126*, e2020JG006000. https://doi.org/10.1029/2020JG006000

Received 31 JUL 2020
Accepted 26 FEB 2021

Author Contributions:

Conceptualization: Marguerite Mauritz, Elaine Pegoraro, Edward A. G. Schuur
Formal analysis: Marguerite Mauritz, Kiona Ogle
Funding acquisition: Edward A. G. Schuur
Methodology: Marguerite Mauritz, Elaine Pegoraro, Edward A. G. Schuur
Resources: Christopher Ebert, Edward A. G. Schuur
Visualization: Marguerite Mauritz
Writing – original draft: Marguerite Mauritz
Writing – review & editing: Elaine Pegoraro, Kiona Ogle, Christopher Ebert, Edward A. G. Schuur

Abstract Isotopic radiocarbon ($\Delta^{14}C$) signatures of ecosystem respiration (Reco) can identify old soil carbon (C) loss and serve as an early indicator of permafrost destabilization in a warming climate. Warming also stimulates plant productivity causing plant respiration to dominate Reco $\Delta^{14}C$ signatures and potentially obscuring old soil C loss. Here, we investigate how a wide spatio-temporal gradient of permafrost thaw and plant productivity affects Reco $\Delta^{14}C$ patterns and isotopic partitioning. Spatial gradients came from a warming experiment with doubling thaw depth and variable biomass, and a vegetation removal manipulation to eliminate plant contributions. We sampled in August and September to capture transitions from high to low plant productivity, decreased surface soil temperature, and relatively small seasonal thaw extensions. We found that surface processes dominate spatial variation in old soil C loss and a process-based partitioning approach was crucial for constraining old soil C loss. Resampling the same plots in different times of the year revealed that old soil C losses tripled with cooling surface temperature, and the largest old soil C losses were detected when the organic-to-mineral soil horizons thawed (~50–60 cm). We suggest that the measured increase in old soil respiration over the season and when the organic-to-mineral horizon thawed, may be explained by mobilization of nitrogen that stimulates microbial decomposition at depth. Our results suggest that soil C in the organic to mineral horizon may be an important source of soil C loss as the entire Arctic region warms and could lead to nonlinearities in projected permafrost climate feedbacks.

1. Introduction

High-latitude soils store 1,460–1,600 Pg carbon (C) and play a critical role in global climate regulation (Hugelius et al., 2014; Schuur et al., 2018; Strauss et al., 2017). A large proportion of the high latitude soil C stock is sequestered in permafrost (Hugelius et al., 2014), ground that remains frozen for at least two consecutive years. Much of the soil C in permafrost is thousands of years old, indicating that for millennia, C inputs exceeded C loss as cold soil conditions limited decomposition (Ping et al., 2015; Pries et al., 2012; Schuur et al., 2008). Carbon loss from permafrost is an important indicator of high-latitude soil carbon stock vulnerability to warming, destabilization, and redistribution of C from soil into the atmosphere (Schuur et al., 2015; Trumbore, 2009; Vonk et al., 2015; Wild et al., 2019). However, it remains unclear on what timescales the Arctic will emerge as a net atmospheric C source due to increasing exposure of ancient soil C stocks (Pries et al., 2012; Schuur et al., 2008; Walter Anthony et al., 2018), or whether increases in summer plant C uptake (McGuire et al., 2016; Meredith et al., 2019) and new peat formation (Heffernan et al., 2020; Jones et al., 2012) will continue to offset losses (Abbott et al., 2016), and to what extent anaerobic conditions (Schädel et al., 2016, 2018; Schuur et al., 2015; Treat et al., 2015) may continue to limit soil C loss.

Permafrost thaw increases soil decomposition rates (Schädel et al., 2014) and simultaneously promotes plant growth (DeMarco et al., 2014; Johansson et al., 2013; Salmon et al., 2016) and plant inputs to surface soil (DeMarco et al., 2014). In the Arctic, the typical metric of ecosystem C loss under field conditions is ecosystem CO_2 respiration (Reco), which measures CO_2 respired from soil microbes and plants due to the low-stature and often continuous cover of vegetation. This contrasts with many other ecosystems where it is possible to nondestructively measure soil respiration in the absence of above-ground plant respiration (Bond-Lamberty et al., 2020; Phillips et al., 2016). However, concomitant increases in plant and surface soil respiration during permafrost thaw (Hicks Pries et al., 2015, 2016) make it impossible to directly

relate thaw-related changes in Reco to increased soil decomposition. Isotopic $\Delta^{14}C$ signatures of Reco can separate contributions from plant, surface soil, and permafrost respiration because permafrost soil C is so much older than the plant and surface soil C pools, producing a very distinct isotopic end-member (Schuur et al., 2009; Trumbore, 2000, 2009). Plant respiration end-members typically have $\Delta^{14}C$ signatures similar to the atmosphere at the time of photosynthetic fixation. Soil C starts with the same $\Delta^{14}C$ signature as plant inputs and gradually ages with depth depending on the rate of soil organic matter turnover. The $\Delta^{14}C$ signature of permafrost soil respiration is very negative because the soil C is old and has undergone notable radioactive decay (Schuur et al., 2009). Atmospheric nuclear testing in the 1960s enriched the atmosphere with ^{14}C, inadvertently creating a label for tracking decadal ecosystem C pools (Trumbore, 2009). As a result, the closer the origin of a C pool is to the 1960s, the more enriched it is in $\Delta^{14}C$. Since testing was halted, atmospheric $\Delta^{14}C$ has been declining due to sequestration of C into ocean and terrestrial ecosystems. Carbon that was incorporated into an ecosystem more recently than the nuclear testing era therefore has a progressively lower $\Delta^{14}C$ signature, such that C fixed by plants this year would have a lower $\Delta^{14}C$ than last year (Schuur et al., 2016). Plant respiration is largely dominated by C fixed in the few preceding years, and can therefore be distinguished from surface soil respiration that contains a larger proportion of ^{14}C-enriched, decadal C. Both plants and surface soil are distinct from very old soil C preserved in permafrost that has undergone radioactive decay (Schuur & Trumbore, 2006; Schuur et al., 2009). Despite the utility of $\Delta^{14}C$ signatures for partitioning ecosystem respiration, challenges arise when the magnitude of flux rates between different sources varies substantially and when end-members overlap. This study addresses the challenge of detecting old soil C respiration from Arctic tundra underlain by permafrost, where plant and surface soil respiration can be so dominant that they obscure the much smaller signal from permafrost soil respiration (Nowinski et al., 2010) and where soil warming and permafrost thaw increase plant and surface-soil respiration to a larger extent than old-soil respiration (Hicks Pries et al., 2016).

This study was conducted at a sub-Arctic moist acidic tundra site where the permafrost temperatures are close to 0°C and highly vulnerable to thaw in the coming decades (Osterkamp et al., 2009; Romanovsky et al., 2017). In this study we use a soil warming manipulation and vegetation removal to investigate how variation in plant and surface soil respiration affect Reco $\Delta^{14}C$ and estimates of old soil respiration. Previous work has shown that at near-peak greenness, when surface soil temperatures and thaw depth are close to the seasonal maximum, Reco $\Delta^{14}C$ was younger and the proportion of old soil C was lower in deeply thawed areas due to rapid increases in plant productivity in the first two years of warming (Hicks Pries et al., 2016). To investigate how plant and young surface soil contributions affect Reco $\Delta^{14}C$ signatures and partitioning of old soil C contributions, we resampled the experiment after five additional years of warming during which plant biomass has doubled (Salmon et al., 2016) and stabilized (Taylor et al., 2018) and thaw has doubled (Mauritz et al., 2017) exposing an estimated total of 70 kg Cm^{-2} of soil C to unfrozen conditions (Plaza et al., 2017).

We use two approaches to maximize variation in plant and young surface soil respiration. Our first approach takes advantage of spatial variation in thaw, plant biomass, and gross primary production (GPP) across the soil warming experiment (Mauritz et al., 2017) and a vegetation removal treatment established in 2012 that represents soil respiration with no direct contribution of plant respiration. In our second approach we sampled at two different time points to capture temporal variation when plant productivity is relatively high (August), and again at the end of the growing season (September) when plant activity is low, and respiration exceeds photosynthesis (net ecosystem exchange measures a net C source) (Mauritz et al., 2017). The decrease in soil temperature between August and September was expected to affect surface soil respiration rates and thus also reduce surface soil contributions in September. Reco was partitioned into plant, young soil, and old soil respiration contributions using a Bayesian isotopic mixing model that incorporated process-based constraints on soil and plant contributions to improve partitioning estimates (Ogle et al., 2016). We hypothesized that: (H1) The flux rate of old soil respiration from vegetation removal plots would remain similar between August and September as seasonal reductions in Reco with cooling surface temperatures are driven by young soil respiration. (H2) Old soil flux rates in vegetated plots will be lower than from vegetation removal plots in August when plant activity is highest and will converge in September when plant contributions are lower because high plant contributions lead to underestimates of old soil contributions to Reco. (H3) Late season sampling will result in a stronger correlation between Reco $\Delta^{14}C$ and thaw because of lower plant activity and maximum extents of thaw depth.

This study contributes to our understanding of how warming impacts the C balance of permafrost ecosystems by systematically examining how variation in young respiration sources (plants and surface soil) affect Reco $\Delta^{14}C$ and inferences about old soil C loss.

2. Materials and Methods

2.1. Site Description

The study site is located in the Carbon in Permafrost Experimental Heating and Drying Research (CiPEHR and DryPEHR) manipulation site at Eight Mile Lake (EML) Watershed, AK, USA (−149.23°W, 63.88°N, 670 m) which occupies traditional land of the Tanana Athabaskan people (Native Land Digital, 2020; Tanana Chiefs Conference, 2020). The site is on a gentle (~3°), northeast-facing slope, underlain by degrading permafrost, in the discontinuous permafrost zone (Osterkamp et al., 2009). Depending on microtopography, the top 30 cm of surface soil can be drained or inundated. Soil organic C content is, on average, 72 kg m^{-2} to 1 m depth (Plaza et al., 2017), and a 0.25–0.40 m thick organic horizon overlies cryoturbated glacial till and loess mineral soils. Mean (±1 s.e.) annual air temperature in the area was −0.94°C ± 0.25°C from 1977 to 2015, with a May–September mean of 11.91°C ± 0.22°C and an October–April mean of −10.09°C ± 0.33°C (Healy and McKinley Stations, Western Regional Climate Center, and NOAA National Centers for Environmental Information). In 2015, the year of study, the May–September mean air temperature was 9.53°C, and October–April mean for 2014/2015 was −8.15°C. The vegetation is typical of moist acidic tundra, dominated by the tussock forming sedge *Eriophorum vaginatum*, the shrubs *Betula nana*, *Vaccinium uliginosum*, and *Vaccinum vitis-ideae*, and mosses *Sphagnum spp*., *Dicranum spp*, and *Pleurozium spp*. (Deane-Coe et al., 2015; Natali et al., 2012; Schuur et al., 2007).

2.2. Experimental Design of Warming Manipulation and Vegetation Removal

The CiPEHR and DryPEHR manipulations were designed to simulate effects of warmer air and soil temperatures, permafrost degradation, and lowered water-table on ecosystem C exchange. Snow fences and snow removal were used to manipulate soil temperatures. The experiment is arrayed in three blocks within 100 m of each other in similar landscape positions, with two replicate snow fences per block. Each snow fence contains 11 plots (0.6 × 0.6 m) that receive different combinations of warming and drying (for details on CiPEHR see Natali et al., 2011, and for DryPEHR, see Natali et al., 2015). For this study we sampled a subset of 7 plots at each fence (48 plots total). Soil warming was initiated in the winter of 2008/2009, air warming in April 2009 (CiPEHR), and water table manipulation in June 2011 (DryPEHR). Briefly, soil warming was achieved using snow fences (1.5 m high × 8 m long) that trap snow down-wind and insulate the soil in the winter; air warming was achieved using polycarbonate open top chambers (cubicle OTCs: 0.36 m^2 × 0.5 m), and drying was controlled by water pumps. Each April, the excess snowpack is manually removed to match the ambient snowpack and to avoid artifacts such as increased water input and delayed phenology (Walker et al., 1999). For ease, we will collectively refer to plots within CiPEHR and DryPEHR as "CiPEHR."

When CiPEHR was launched in 2008, maximum seasonal thaw was around 0.5 m and water tables were below the soil surface, by 2015 maximum thaw depths were up to 1 m in experimental soil warming plots (Mauritz et al., 2017). Over time, heterogeneous thaw and ground surface subsidence has created different thaw and moisture trajectories resulting in plots that range from shallow thaw and dry conditions to deep thaw and wet conditions (Figure S1). Over the 2009–2015 period, effects of air warming on CO_2 fluxes (e.g., Reco) have been small and nonsignificant (Mauritz et al., 2017).

Vegetation removal plots (total 6 plots; 0.6 × 0.6 m) were established in July 2012. Vegetation removal plots are 500 m away from the warming manipulation and subject only to ambient climate conditions. Vegetation removal plots were trenched to 30 cm with plastic sheeting and all vascular vegetation and non-vascular photosynthetic area was clipped at the surface; these plots have been maintained by regular clipping, with little or no re-sprouting observed in the year of sampling.

2.3. Environmental and Vegetation Measurements

At CiPEHR, plot-level environmental and vegetation variables were measured in paired plots immediately adjacent to each Reco $\Delta^{14}C$ sampling plot (described below). In the vegetation removal plots, all data were collected in the same plots as Reco $\Delta^{14}C$ sampling. Soil temperatures were measured half-hourly at 5, 10, 20, and 40 cm depths at CiPEHR and at 5 and 10 cm in vegetation removal plots (in 2016 and 2017) using type T copper-constantan thermocouples. Soil temperatures for vegetation removal plots in 2015 were estimated from 2015 air temperatures measured continuously at the site, using plot- and depth-specific relationships between air and soil temperatures in 2017. Soil temperature profiles deeper than 40 cm (maximum continuous measurement depth) were linearly interpolated to 1 m depth on all days that thaw depth was deeper than 40 cm using the plot-specific soil temperature measurements up to 40 cm. We assumed that frozen soil was −0.2°C, the soil temperature at 1 m (Salmon et al., 2018; Figure S2).

Water table depth (WTD) was measured twice a week within the CiPEHR footprint as in Vogel et al. (2009). WTD was assigned to each Reco $\Delta^{14}C$ plot based on proximity to WTD wells because WTD was not measured within each plot. At the vegetation removal plots, WTD was not measured so the four plots with water visible at the surface all season were assigned WTD = 0 cm. Two plots did not have water visible at the surface and we assumed WTD = −10 cm which represents an average WTD for the site as a whole and we believe is a reasonable characterization based on weekly visits to the vegetation removal plots and strong familiarity with the site. We tested the effect of changing the assumption of WTD to a much shallower water table (−2 cm) or much deeper (−20 cm) on the model fit of the final regression model and found a relatively small effect (see Section 4.2).

Thaw depth (TD) was measured the week of each Reco $\Delta^{14}C$ measurement. Plot-level plant activity for CiPEHR plots is represented by gross primary productivity (GPP) estimates from automated chamber measurements (0.36 $m^2 \times 0.5$ m tall for air warming and 0.25 m tall and constantly ventilated for plots with no air warming) on paired plots immediately adjacent to Reco $\Delta^{14}C$ plots (Hicks Pries et al., 2016; Mauritz et al., 2017). For the vegetation removal plots, GPP = 0, reflecting the absence of photosynthesizing plants. The mean value of plot-specific soil temperature, TD, WTD, and GPP for seven days preceding each Reco $\Delta^{14}C$ sampling point were used in subsequent statistical models that relate (or partition) Reco $\Delta^{14}C$ to these driving variables.

2.4. Ecosystem Respiration $\Delta^{14}C$ Measurements

Ecosystem respiration was sampled in early August and early September 2015 using previously installed PVC collars (25.4 cm diameter, 10 cm high, 6–7 cm deep in the ground) and established methods for this site (Hicks Pries et al., 2013, 2016; Natali et al., 2015). A total of 27 plots were sampled each month (CiPEHR, $n = 21$; vegetation removal, $n = 6$). All field sampling took place early in the morning under calm atmospheric conditions to control for potential diurnal variation and diffusion changes associated with atmospheric turbulence. Chamber headspace $\Delta^{14}C$ was sampled with 10L dark chambers fitted onto the collars to encompass all aboveground biomass, when present. After placement, the chamber headspace was scrubbed with soda lime. Flow rates during scrubbing were adjusted to approximately match respiration rates and ambient pCO_2 concentrations in the chamber headspace and avoid a strong negative CO_2 gradient from soil to headspace (following Gaudinski et al., 2000). After 45 min of scrubbing, chamber air was circulated through a zeolite molecular sieve trap (Alltech 13X, Alltech Associates) for 15 min to collect respired CO_2. Total Reco flux rates were measured directly from the $\Delta^{14}C$ sampling collars using a Picarro G2121i analyzer during the same week of measurement (Mauritz et al., 2018). All flux rates were converted from concentration to mass (μmol CO_2 $m^{-2}sec^{-1}$) using plot-specific chamber volumes, and air temperature and atmospheric pressure at the time of measurement from a meteorological tower at CiPEHR.

For $\Delta^{14}C$ analysis, the molecular sieves were baked at 625°C to desorb CO_2 (Bauer et al., 1992), desorbed CO_2 was cryogenically purified on a vacuum line, sub-sampled for $\delta^{13}C$ and then reduced to graphite by Fe reduction in H_2 (Vogel et al., 1987). Graphite was analyzed for ^{14}C content at the UC Irvine W.M. Keck Carbon Cycles Accelerator Mass Spectrometry (AMS) Laboratory (precision ± 2‰–3‰). Final values of Reco $\Delta^{14}C$ are reported following a sample-specific correction for mass dependent fractionation effects and for potential incursion of atmospheric air due to lateral diffusion into the chamber headspace or system

leaks during sampling. These corrections use the sample-specific $\delta^{13}C$ in a two-pool mixing model with atmospheric $\delta^{13}C$ at the time of measurement and a site-specific estimate of soil-respired $\delta^{13}C$, following standard procedure (Gaudinski et al., 2000; Schuur et al., 2009). Based on 10 years of sample analysis, atmospheric CO_2 in samples that pass quality control is less than 16% of the total sample volume (Chris Ebert, pers comm).

2.5. Plant and Soil $\Delta^{14}C$ End-Member Incubations

Plant and soil end-member data come from previous studies at the site (Hicks Pries et al., 2013, 2016; Schuur et al., 2009). Plant end-members were measured at EML in 2004 (at ambient conditions) and during each year from 2008 to 2011 (from CiPEHR). Above- (AG) and below-ground (BG) tissues were harvested and immediately placed in dark incubation jars. The jar headspace was briefly scrubbed using soda lime to remove atmospheric CO_2, respired CO_2 was allowed to accumulate for 4 h, and headspace was sampled with molecular sieve traps (section 2.4). For plant-free soil respiration end-member incubations, surface soils (0–25 cm) were collected in 2009 and 2010 and deep cores (25–75 cm) were collected in 2010 (from CiPEHR: Hicks Pries et al., 2016). Prior to incubation shallow and deep soil cores were sectioned into 10 cm depth increments and all roots >1 mm were removed. Soil samples were allowed to sit at room temperature to eliminate recent root-derived (autotrophic) C contributions and then incubated at field soil moisture capacity and in aerobic conditions. Soil (heterotrophic) flux rates were measured during three short (~3 h) incubations. For $\Delta^{14}C$ sampling, the headspace was scrubbed, CO_2 allowed to accumulate to 1.5 mg C (12–72 h) and sampled on molecular sieve traps (Section 2.4). For the partitioning model (Sections 2.7.1 and 2.7.2), plant end-members were treated as replicates regardless of treatment, and soil-endmembers were averaged by control or soil warming for each fence and each year and pooled as individual replicates (=12 values per year for each young and old soil end-member) following Hicks Pries et al. (2016). Carbonates have a negligible effect on soil-respired $\Delta^{14}C$ based on the acidity of soils at this site which precludes carbonate formation (pH 4.5–5.2 from surface to 55 cm depth; Bracho et al., 2016) and the absence of carbonates has additionally been confirmed through soil tests (Elaine Pegoraro, pers comm).

2.6. Regression Model to Identify Factors Influencing Reco $\Delta^{14}C$

We used linear regression analyses in a Bayesian framework to identify drivers of Reco $\Delta^{14}C$, which we subsequently used to inform the process-based partitioning model (section 2.7). Following informal, preliminary model comparison, we regressed observed Reco $\Delta^{14}C$ values ($\Delta^{14}C^{Reco}$) on meaningful combinations of environmental variables and associated 2- and 3-way interactions. For each observation i (all plots in August and September, $i = 1, 2, ..., 96$), the observed $\Delta^{14}C^{Reco}$ were assumed to be normally distributed around a mean, μ^{Reco}, which was defined by normalized covariates at time of sampling: GPP, WTD, surface soil temperature (T), and thaw depth (TD) and all 2-way interactions. The only 3-way interaction was GPP*T*TD which reflects the experimental design of vegetation removal (GPP), thaw gradients (TD), and seasonal variation reflected most strongly in surface soil temperature (T) and GPP. Other 3-way interactions were excluded to avoid an overly complex model, particularly for the partitioning model (Section 2.7). The regression model is expressed:

$$\Delta^{14}C_i^{Reco} \sim \text{Normal}\left(\mu_i^{Reco}, \sigma^2_{Reco}\right) \tag{1}$$

$$\begin{aligned}\mu_i^{Reco} = {} & \alpha_1 + \alpha_2 GPP_i + \alpha_3 WTD_i + \alpha_4 T_i + \alpha_5 TD_i + \alpha_6 GPP_i WTD_i + \alpha_7 GPP_i TD_i \\ & + \alpha_8 GPP_i T_i + \alpha_9 WTD_i TD_1 + \alpha_{10} WTD_i T_i + \alpha_{11} TD_i T_i + \alpha_{12} GPP_i TD_i T_1\end{aligned} \tag{2}$$

within the Bayesian framework, we assigned standard, relatively non-informative priors to the regression coefficients (α terms) and the residual error variance (σ^2_{Reco}; Text S1 and Section 2.7).

2.7. Process-Based Partitioning Model

The relative contributions of CO_2 derived from plant, young soil, and old soil sources to Reco were estimated using a Bayesian modeling approach that combines (a) a single plant end-member model, (b) a

season-specific temperature adjusted soil end-member model, (c) a three-pool isotope partitioning model, and (d) environmental drivers governing the contribution of old soil CO_2 relative to other sources. Combining these four sub-models into one model allows propagation of uncertainty due to observation or measurement errors, parameter uncertainty, and inherent variability of individual biological processes. To ensure realistic error propagation we controlled feedback among sub-models using the cut function available within OpenBUGS (Lunn et al., 2009; Ogle et al., 2013). This feedback control allowed uncertainty associated with end-member estimates to be propagated to the partitioning model, while preventing the portioning model from feeding back to unduly influence end-member estimates (Ogle & Pendall, 2015). The structure of the model is illustrated in Figure 1 and described below.

2.7.1. End-Member Models

The plant $\Delta^{14}C$ end-member for 2015 was estimated assuming a linear decline in $\Delta^{14}C$ over time based on the above- (AG) and below- (BG) ground plant respired $\Delta^{14}C$ measured in 2004 and 2008–2011 (Hicks Pries et al., 2013, 2016; Schuur et al., 2009). Plant end-member respiration ($\Delta^{14}C^{Plant}$) was modeled as the mixed signal of AG and BG respiration using individual AG and BG observations (Table S4). Plant respiration of the local tundra shrubs, graminoids, and mosses consists primarily of current year photosynthate (Hicks Pries et al., 2013) and the plant end-member is expected to become more depleted in $\Delta^{14}C$ over time as atmospheric $\Delta^{14}C$ decays. Thus we use a linear regression to predict $\Delta^{14}C^{Plant}$ in 2015 and for each observation $\Delta^{14}C^{Plant}$ (AG and BG) i (i = 1,2, ..., 18) in this data set we assume:

$$\Delta^{14}C_i^{Plant} \sim \text{Normal}\left(\mu_i^{Plant}, \sigma^2_{Plant}\right) \tag{3}$$

$$\mu_i^{Plant} = \beta_0 + \beta_1\left(\text{year}_i - 2004\right) \tag{4}$$

where σ^2_{Plant} describes the variability among all plant end-members. The intercept (β_0) is defined as the plant end-member in 2004 and the slope (β_1) is the annual rate of change in $\Delta^{14}C^{Plant}$. Thus, the estimated plant end-member for 2015 used in the isotopic mixing model (Equation 8) is given by $\mu_{2015}^{Plant} = \beta_0 + \beta_1\left(2015 - 2004\right)$.

The young and old soil respiration end-members for 2015 were calculated as the integrated surface (0–25 cm) = young and deep (25–75 cm) = old soil $\Delta^{14}C$ respiration. To get a representative $\Delta^{14}C$ value for soil respiration in the field, the respiration rates of each 10 cm depth were temperature corrected using depth-specific field temperatures from 2015 and Q_{10} = 2.6 (Bracho et al., 2016; Hicks Pries et al., 2013). The integrated young and old soil end-members were then calculated as the weighted relative contribution from each layer resulting in 12 replicate observations (Table S7 and S8). The surface (i = 1, 2, ..., 12) and deep (i = 1, 2, ..., 12) soil $\Delta^{14}C$ respiration for each field core sample were treated as replicate observations and assumed to follow a normal distribution, with means representing the end-member values of young and old soil (μ^{Young} and μ^{Old}, respectively). The soil $\Delta^{14}C$ end-member was assumed to vary by sample date to reflect the influence of seasonal declines in field soil temperature from August to September (Table 1):

$$\Delta^{14}C_i^{Young} \sim \text{Normal}\left(\mu_{D(i)}^{Young}, \sigma^2_{Young}\right) \tag{5}$$

$$\Delta^{14}C_i^{Old} \sim \text{Normal}\left(\mu_{D(i)}^{Old}, \sigma^2_{Old}\right) \tag{6}$$

where $D(i)$ denotes the sample date associated with observation i, and σ^2_{Young} and σ^2_{Old} describe the variability among the core-level integrated soil respiration $\Delta^{14}C$ values within each sampling date.

2.7.2. Partitioning Model

We used a three-source isotope mixing model to estimate plot-level proportional contributions of plant (P^{Plant}), young soil (P^{Young}), and old soil (P^{Old}) to ecosystem respiration. The plot-level observed $\Delta^{14}C^{Reco}$ is assumed follow a normal distribution with mean, μ, and variance, σ^2:

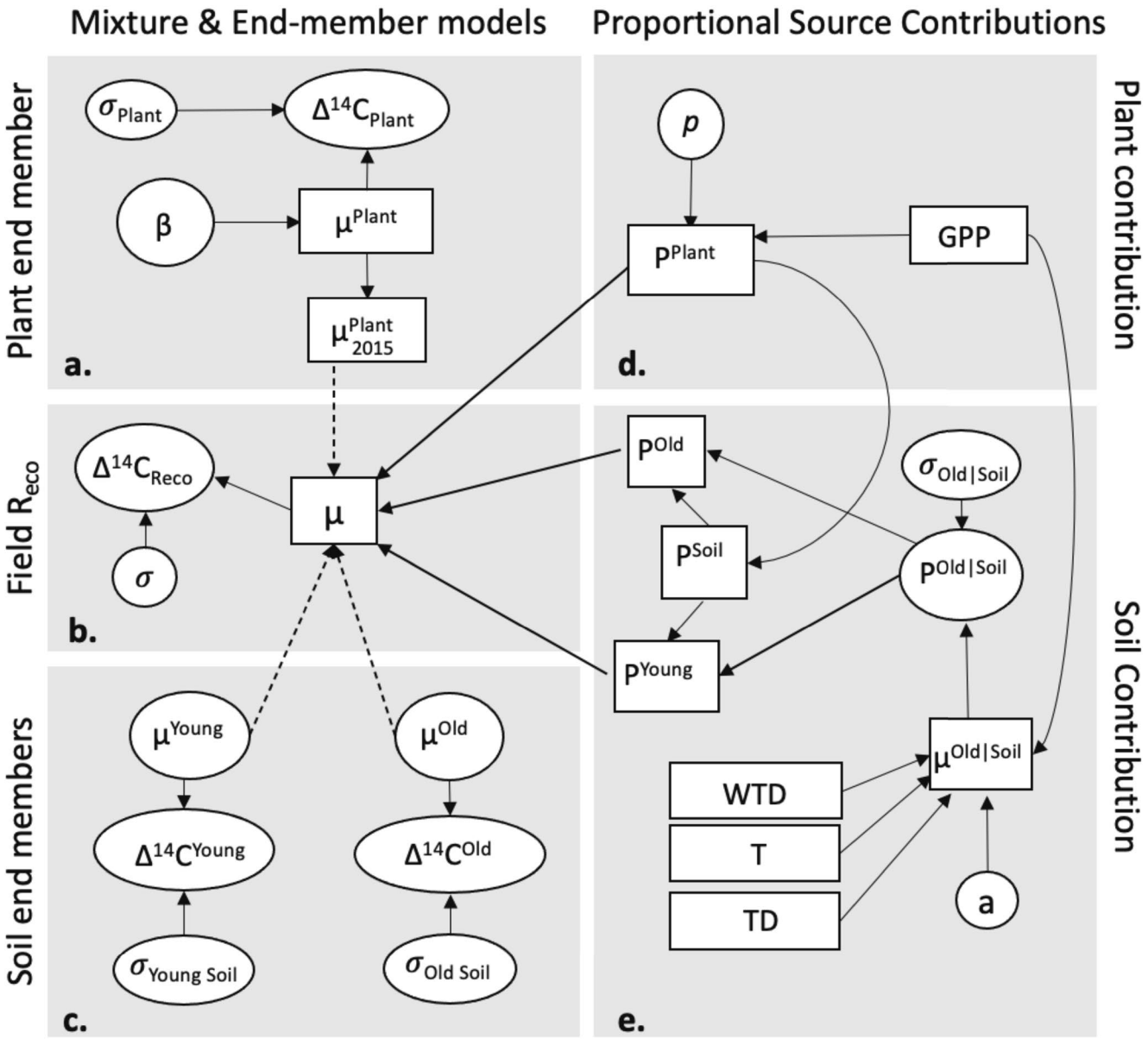

Figure 1. Graphical representation of the sub-models for partitioning Reco. (a) The plant end-member (μ^{Plant}) was estimated for the year of this study (2015) assuming linear decay of plant $\Delta^{14}C$ over time (Section 2.7.1, Equation 3). (c) Soil end-members (μ^{Young} and μ^{Old}) were estimated for each sample date using field temperature-adjusted soil incubation data (Section 2.7.1, Equations 5 and 6). (b) The predicted plot-level Reco $\Delta^{14}C$ (μ) (Section 2.7.2, Equations 7 and 8) was modeled via a process-based mixing model that depends on the end-member isotopic signatures and the relative contributions from (d) plant respiration (Section 2.7.2, Equation 10) and (e) young and old soil respiration (Section 2.7.2, Equation 11). The process-based model included sub-models for the relative contributions from young and old soil (P^{Young} and P^{Old}) modeled as a function of gross primary productivity (GPP), water table depth (WTD), integrated surface soil temperature from 0-10 cm (T), and thaw depth (TD) (Section 2.7.2, Equations 12 and 13). (d) The plant contribution (P^{Plant}) was constrained by plot-level GPP and used in the determination of P^{Soil} (Section 2.7.2, Equations 8 and 9). The isotopic end-member estimates were "cut" so that information flow is unidirectional and the field Reco $\Delta^{14}C$ and mixing model do not feedback to the end-member models (shown with dashed lines). Circular nodes indicate stochastic quantities that were assigned distributions; square nodes are either fixed measurement values or deterministic functions of other quantities. The μ terms indicate model means, β and α refer to regression parameters for μ^{Plant} and $\mu^{Old|Soil}$, respectively, p is a scalar that constrained P^{Plant} based on GPP, and the σ terms quantify different sources of error or uncertainty.

Table 1
Environmental Conditions, GPP, and Reco Flux Rates for Vegetated and Vegetation Removal Plots in August and September of 2015

		Vegetated (veg)			Vegetation removal (no veg)		
Variable	Month	Mean	Max	Min	Mean	Max	Min
Water table depth	August	−11	11	−32	−3	0	−10
(WTD, cm)	September	−11	5	−31	−3	0	−10
Thaw depth	August	68	96	46	53	59	50
(TD, cm)	September	76	111	55	61	67	55
Surface soil temperature (5 and 10 cm)	August	7.65	9.11	6.27	9.39	10.37	8.03
(T, °C)	September	3.20	4.10	2.66	3.67	4.03	3.27
Deep soil temperature (40 cm to thaw depth)	August	0.32	1.41	−0.17	−0.01	0.14	−0.11
(°C)	September	0.21	1.09	−0.09	−0.07	0.06	−0.07
GPP flux rate	August	3.95	7.33	1.92	0.00	0.00	0.00
(μmol CO2 m^{-2} s^{-1})	September	0.90	1.71	0.27	0.00	0.00	0.00
Reco flux rate	August	3.26	7.24	1.48	1.36	2.70	0.89
(μmol CO2 m^{-2} s^{-1})	September	1.80	2.95	0.80	0.77	1.11	0.36

Note. The water table can be above or below the soil surface so positive values for WTD indicate standing water and negative values indicate depth to the water table below the soil surface. Thaw depth (TD) is the depth from the soil surface to the top of the frozen soil layer, reported as a positive value. Mean, maximum, and minimum values are reported the week prior to Reco $\Delta^{14}C$ sampling.
GPP, gross primary productivity.

$$\Delta^{14}C_i^{Reco} \sim \text{Normal}\left(\mu_i, \sigma^2\right) \tag{7}$$

A standard mixing model was used to define the mean or predicted $\Delta^{14}C^{Reco}$, μ, given the plant, young soil, and old soil end-members (μ^{Plant}, μ^{Young}, and μ^{Old}, respectively), with the two soil end-members varying by sample date. Thus, the mixing model for μ is given by:

$$\mu_i = P_i^{Plant}\mu^{Plant} + P_i^{Young}\mu_{D(i)}^{Young} + P_i^{Old}\mu_{D(i)}^{Old} \tag{8}$$

where, again, $D(i)$ indicates sampling date, D, associated with each $\Delta^{14}C^{Reco}$ observation i. Importantly, the end-members are estimated from their corresponding data, based on Equations 3–8, and the values of μ^{Plant}, μ^{Young}, and μ^{Old} are "cut" before supplying them to the mixing model in Equation 8 so that information flow is unidirectional and the field Reco $\Delta^{14}C$ and mixing model do not feedback to the end-member models (Ogle & Pendall, 2015).

Next, we define models for the relative contributions that incorporate the effects of environmental and plant covariates. We use a simple model for P^{Plant} that assumes the contribution of plant respiration is proportional to plant activity, as indicated by the observed GPP data:

$$P_i^{Plant} = p\text{GPP}_i \tag{9}$$

Here, p is a scaling factor between 0 and $1/\text{GPP}_{max}$, where GPP_{max} is the maximum observed GPP, thus constraining P^{Plant} between 0 and 1.

The three relative contributions must add to one, such that the total soil (young + old) contribution is given by:

$$P_i^{Soil} = 1 - P_i^{Plant} \tag{10}$$

From P^{Soil} we can denote $P^{Old|Soil}$ as the contribution of the old soil to the total soil contribution, and determine the relative contributions from young (P^{Young}) and old (P^{Old}) soil:

$$P_i^{\text{Old}} = P_i^{\text{Soil}} * P_i^{\text{Old|Soil}}$$
$$P_i^{\text{Young}} = P_i^{\text{Soil}}\left(1 - P_i^{\text{Old|Soil}}\right). \quad (11)$$

We assumed that the contributions of old and young soil respiration varied in response to soil environmental conditions and plant/root activity. Specifically, we added controls over soil contributions by modeling $P^{\text{Old|Soil}}$ as a function of the covariates identified as important drivers of Reco Δ^{14}C (section 2.6). To constrain $P^{\text{Old|Soil}}$ between 0 and 1, we modeled it on the logit scale, via a normal distribution that accounted for plot-level random effects:

$$\text{Logit}\left(P_i^{\text{Old|Soil}}\right) \sim \text{Normal}\left(\mu_i^{\text{Old|Soil}}, \sigma^2_{\text{Old|Soil}}\right) \quad (12)$$

where i is one plot and $\sigma^2_{\text{Old|Soil}}$ describes the residual plot-level variability of logit scale old soil contributions relative to the total soil contribution. The expected or predicted relative contribution of (logit scale) old soil was regressed on the covariates of GPP, WTD, T, and TD with interactions motivated by the simplified form of Equation 2 (Section 2.6, Table S1), giving:

$$\mu_i^{\text{Old|Soil}} = a_1 + a_2\text{GPP}_i + a_3\text{WTD}_i + a_4\text{T}_i + a_5\text{TD}_i + a_6\text{GPP}_i\text{TD}_i + a_7\text{GPP}_i\text{T}_i + a_8\text{T}_i\text{TD}_i + a_9\text{GPP}_i\text{TD}_i\text{T}_i \quad (13)$$

2.8. Old Soil Respiration Flux Rates

To evaluate the spatial and seasonal changes in old soil C loss, we calculated the plot-level magnitude of old soil respiration (P^{Old} * total Reco). The drivers of old soil flux rate were evaluated using the same regression analysis approach used for total Reco Δ^{14}C (Section 2.6).

2.9. Model Implementation and Evaluation

To complete the model specification associated with Equations 1–13, we assigned priors to all remaining parameters, including all standard deviation terms (i.e., σ_{Reco}, σ_{Plant}, σ_{Young}, σ_{Old}, σ, and $\sigma_{\text{Old|Soil}}$), end-member related effects or means (β_0, β_1, μ_D^{Young}, and μ_D^{Old}), and all coefficients or effects in the regression and partitioning models (α_1, ..., α_{12}, p, a_1, ..., a_9). We used fairly typical and relatively non-informative priors (see Text S2 for the specific priors we used). The models were implemented in the Bayesian software OpenBUGS (Lunn et al., 2000) via the R2OpenBUGS package (Sturtz et al., 2005). Feedback among sub-models was controlled with the cut function (Lunn et al., 2009; Ogle & Pendall, 2015; Ogle et al., 2014). Code is provided in Text S1 (for the regression model given by Equations 1 and 2) and Text S2 (for the partitioning model, Equations 3–13). For each model, 3 parallel Markov Chain Monte Carlo (MCMC) sequences were simulated for a sufficient number of iterations (ca. 1×10^6) to ensure convergence, which was evaluated via the Gelman and Raftery diagnostics (Gelman, 2004) and by visual examination of the sequences (e.g., history plots). The sequences were thinned to reduce within sequences autocorrelation and memory demands, Posterior statistics of means and 95% credible intervals (CI) were computed based on 50,000 post burn-in samples simulated from the posterior distribution of the model parameters.

Model fit was evaluated by comparing observed versus predicted (Gelman, 2004) $\Delta^{14}\text{C}^{\text{Reco}}$ values for the Reco Δ^{14}C models, and plant respired $\Delta^{14}\text{C}^{\text{Plant}}$ for the plant-end-member sub-model (Figure S3 and S4).

2.10. Model Selection

The simplest, best fitting models for the regression (Equations 1 and 2) and partitioning models (Equations 3–13) were arrived at by evaluating the effect of removing variables (covariates) on changes in the deviance information criterion (DIC; Spiegelhalter et al., 2002) and its associated penalty term (pD, the effective number of parameters), posterior predictive loss (Dsum; Gelfand & Ghosh, 1998), and the coefficient of determination (R^2) from regressions of observed versus predicted values. Model selection was implemented by iteratively removing one variable, starting with the most complex interaction term and

redefining a reduced model before further removing lower order terms. During model development we determined that TD was a slightly better predictor than deep soil temperature, so we retained TD in our final set of models; TD and deep soil temperatures are also correlated (Figure S1). The simplest model from the $\Delta^{14}C^{Reco}$ regression model (Equations 1 and 2) motivated the specification of Equation 13 in the more complex mixing model because source partitioning depends on variation in $\Delta^{14}C^{Reco}$.

3. Data Archive

All data, as used in this manuscript, are printed in Tables S4–S8 and the complete datasets are archived in the Bonanza Creek LTER Data Catalog (Table S9).

4. Results

4.1. Spatial and Temporal Plot Conditions

Environmental conditions were much more spatially variable in vegetated plots (Veg, or CiPEHR) compared to vegetation removal plots (No Veg; Table 1) due to the experimental soil warming manipulation at CiPEHR which greatly expanded the environmental envelope (Figure S1a). On average, vegetated plots were drier and more deeply thawed than vegetation removal plots (Table 1 and Figure S1a). Surface soil temperatures were slightly cooler in vegetated than in vegetation removal plots in August but not in September (Table 1). Deep soil temperatures were warmer in vegetated than vegetation removal plots, mostly due to an increase in the maximum temperature (Table 1). Deep soil temperatures were positively correlated with TD, which is to be expected since warmer temperatures lead to thaw (Figure S1b).

Seasonal changes in mean conditions from August to September followed similar patterns in vegetated and vegetation removal plots. From August to September the mean TD increased on average 10 cm and surface soil temperatures declined by 5°C–6°C while mean water table depth and deep soil temperatures remained similar (Table 1). In vegetation removal plots, GPP = 0 and Reco flux rates were on average half as large as Reco flux rates in vegetated plots. From August to September GPP declined on average 76% in vegetated plots and Reco fluxes declined by 56% in both vegetated and vegetation removal plots (Table 1).

4.2. Reco $\Delta^{14}C$ Patterns and Controls

The Reco $\Delta^{14}C$ signature differed between August and September and between vegetated and vegetation removal plots (Figures 2a and 2b). In August, vegetation removal plots supported the highest measured Reco $\Delta^{14}C$, ranging from 37‰ to 73‰ (Figures 2a and 2b), close to the young soil end-member (Figure 2c). Reco $\Delta^{14}C$ in vegetated plots ranged from −12‰ to 67‰ with most plots showing values between the plant (23‰) and young soil (71‰) end-members. In September, the Reco $\Delta^{14}C$ signatures of each plot became more negative, shifting closer to the old soil end-member (−180‰). The most negative Reco $\Delta^{14}C$ were from vegetation removal plots during September (−34‰ to −173‰), and the Reco $\Delta^{14}C$ from vegetated plots ranged from 53‰ to −110‰, with many of the Reco $\Delta^{14}C$ values just below the atmospheric signature (18.3‰).

The regression model in Equation 2 explained 45% of the variation in Reco $\Delta^{14}C$ and helped to identify potentially important drivers of Reco $\Delta^{14}C$. Across all plots and sampling times, Reco $\Delta^{14}C$ depended more on GPP than TD with the effects of GPP moderated by surface soil temperature (T) and TD (significant GPPxTxTD interaction; Table 2 and Table S1). In the vegetation removal plots where there was no plant respiration (GPP = 0) Reco $\Delta^{14}C$ was highest in August and became very negative in September (Figure 2a). This large decline in Reco $\Delta^{14}C$ in September in vegetation removal plots coincides with a decline in surface temperature (T, Table 1). When plants were present (GPP > 0) Reco $\Delta^{14}C$ typically decreased as GPP decreased (Figure 2a). In September Reco $\Delta^{14}C$ was also distinctly lower in vegetated plots after an overall decline in GPP with vegetation senescence and cooler soil temperatures (Figure 2a and Table 1).

Across a range of TD from 46 to 110 cm, the effects of TD on Reco $\Delta^{14}C$ were weak. Instead, at any given TD, Reco $\Delta^{14}C$ was typically lower in September than in August (Figure 2b). The most negative Reco $\Delta^{14}C$ was measured in plots with TD = 60–70 cm TD, and these plots also had the lowest GPP and coolest soil temperatures (Figures 2a and 2b).

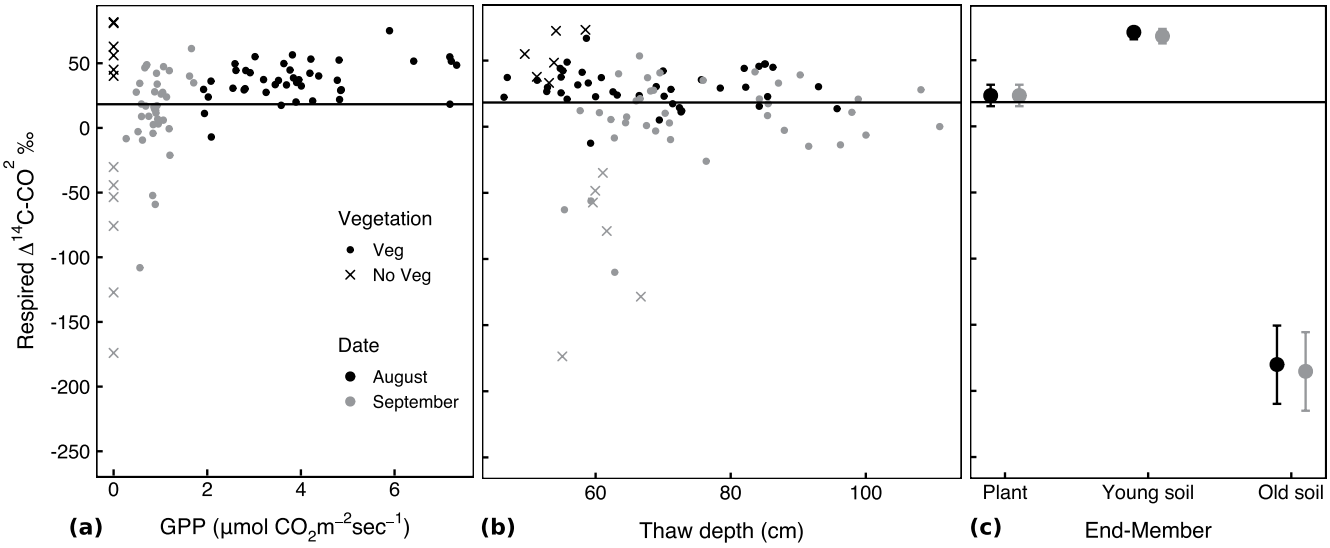

Figure 2. Respired $\Delta^{14}C$-CO_2 (Reco $\Delta^{14}C$) in relation to (a) gross primary productivity (GPP) and (b) thaw depth (TD) from vegetated CiPEHR (Veg) and vegetation removal (No Veg) plots in August and September. (c) End-member values for plant, young, and old soil generally encompass the range of measured Reco $\Delta^{14}C$. In each panel, the horizontal line at 18.3‰ shows the atmospheric $\Delta^{14}C$-CO_2 value in 2015.

The best fitting model for describing variation in Reco $\Delta^{14}C$ included a significant negative effect of WTD on Reco $\Delta^{14}C$ (Table 2), indicating that across a range of WTD from −32 to 11 cm, Reco $\Delta^{14}C$ was more positive when water table depths were lower (i.e., drier surface soil). Changing the assumption of WTD for the two non-saturated vegetation removal from −10 cm to a much shallower water table (−2 cm) or much deeper (−20 cm) had little effect on the model fit of the final regression model (Table S1). Assuming WTD = -2 cm had essentially no effect on the model result, increasing the effect size by one point from −18 (CI: −2.1 to −34.1, Table 2) to −19 (CI: −35 to −4.3). Assuming WTD = −20 cm caused the effect size to decrease to −13 (CI: 7.4 to −27) and go from marginally significant to nonsignificant. Despite the change when assuming WTD = −20 cm the implication of the results is the same: WTD was important for the overall fit of the reduced model with a weak negative effect on Reco $\Delta^{14}C$.

Table 2
Estimated Posterior Mean and 95% Credible Interval (CI) for the Final Regression Parameters Used for $\Delta^{14}C^{Reco}$ Model (Table S1) Based on a Model Selection Process That Began With the Full Model in Equation 2

Best-fit model: $\mu^{Reco} = a_1GPP + a_2WTD + a_3T + a_4TD + a_5GPP*TD + a_6GPP*T + a_7T*TD + a_8GPP*T*TD$

Covariate	Effect	Mean	2.5% CI	97.5% CI
Intercept	α_1	22.0	10.1	33.8
GPP	α_2	**37.0**	**8.8**	**65.8**
WTD	α_3	**−18.0**	**−34.1**	**−2.1**
T	α_4	13.2	−13.7	39.8
TD	α_5	2.0	−19.4	23.5
GPP*TD	α_7	−56.2	−111.4	0.1
GPP*T	α_8	**−74.0**	**−132.4**	**−15.8**
T*TD	α_{11}	7.6	−43.4	58.3
GPP*T*TD	α_{12}	**124.4**	**15.2**	**234.6**

Note. The final model included all covariates shown; covariates in bold had a significant effect on Reco $\Delta^{14}C$ values (i.e.: 95% CI for their effect parameter did not contain zero), all parameter values are effect size of standardized variables. GPP, gross primary productivity; TD, Thaw depth.

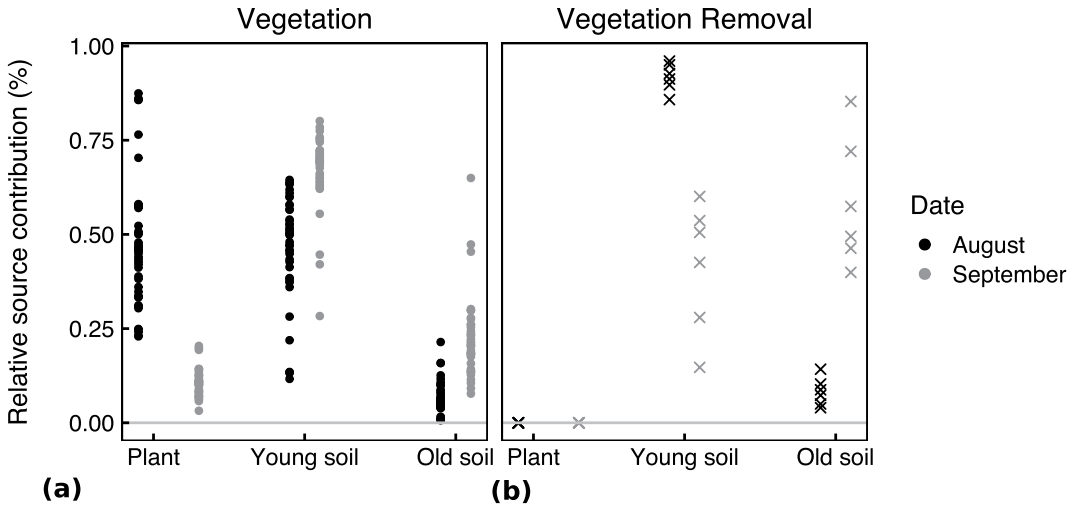

Figure 3. Estimated posterior means of the relative plant (P^{Plant}), young soil (P^{Young}), and old soil (P^{Old}) respiration contributions in (a) vegetated and (b) vegetation removal plots in August (black) and September (gray).

4.3. Predicted End-Member Values

The mean end-member values for plants, young, and old soil were estimated from data-driven sub-models within the partitioning model (Section 2.7.1, Figure 1). The plant end-member sub-model sufficiently described the observed plant respired $\Delta^{14}C$ data ($R^2 = 0.82$, Figure S3) and the predicted plant respired $\Delta^{14}C$ value in 2015 was 23 ‰ (μ^{Plant}_{2015}, Equation 4; Figure 2c and Table S2). Plant respired $\Delta^{14}C$ was always slightly higher than atmospheric $\Delta^{14}C$, and from 2004 to 2009, plant respired $\Delta^{14}C$ declined at a rate of -4‰ year^{-1}, similar to the atmospheric decline (Figure S3). Young and old soil $\Delta^{14}C$ end-members varied seasonally due to differences in soil temperature that altered the relative respiration rates from each soil layer (Table S2, Table 1). Young soil $\Delta^{14}C$ end-members (μ^{Young}, Equation 5) were estimated at 71‰ in August and 68‰ in September (Figure 2c and Table S2), reflecting the decadal nature of young soil C pools. Old soil $\Delta^{14}C$ end-members (μ^{Old}, Equation 6) were very negative, with posterior means of -180‰ in August and -185‰ in September (Figure 2c and Table S1), reflecting the presence of mainly millennial C at deeper depths.

4.4. Relative Contributions of Different Respiration Sources

The partitioning model had a high model fit with evenly distributed uncertainty (95% CI) that indicates the model predicts equally well across the whole data range (μ_i predicted vs observed $R^2 = 0.95$, Figure S4). The partitioning model estimated higher old soil contributions in September than in August for both vegetated and vegetation removal plots (Figure 3). In August the estimated old soil contributions were similar in vegetated (posterior means for P^{Old} ranged from 0% to 21%) and in vegetation removal plots (P^{Old} ranged from 4% to 14%). In September a larger proportion of respiration was attributed to old soil in vegetation removal plots (P^{Old} ranged from 40% to 85%) compared to vegetated plots (P^{Old} ranged from 8% to 65%). The seasonal increase in old soil respiration was accompanied by a decrease in plant respiration from vegetated plots (Figure 3a, P^{Plant} ranged from 23% to 88% in August, declining to 3%–20% in September) and a decrease in young soil respiration from vegetation removal plots (Figure 3b, P^{Young} ranged from 86% to 96% in August, declining to 15%–60% in September). In vegetated plots, P^{Young} increased slightly from August to September, in contrast to the large P^{Young} decline in vegetation removal plots. The very large seasonal P^{Young} decline in vegetation removal plots highlights the importance of surface soil temperature for controlling the contribution of respiration from the young surface soil.

To understand how old soil Reco contributions vary with plant productivity and thawed soil depth, we examined the relationships between P^{Old} versus GPP and TD. The estimated P^{Old} values were lowest in plots with the highest GPP, increased with declining plot-level GPP in August, and increased again as GPP in all plots declined in September (Figure 4a). Across a thaw depth range from 46 to 110 cm, there was no trend toward higher old soil contributions from more deeply thawed plots (Figure 4b). The contribution of P^{Old}

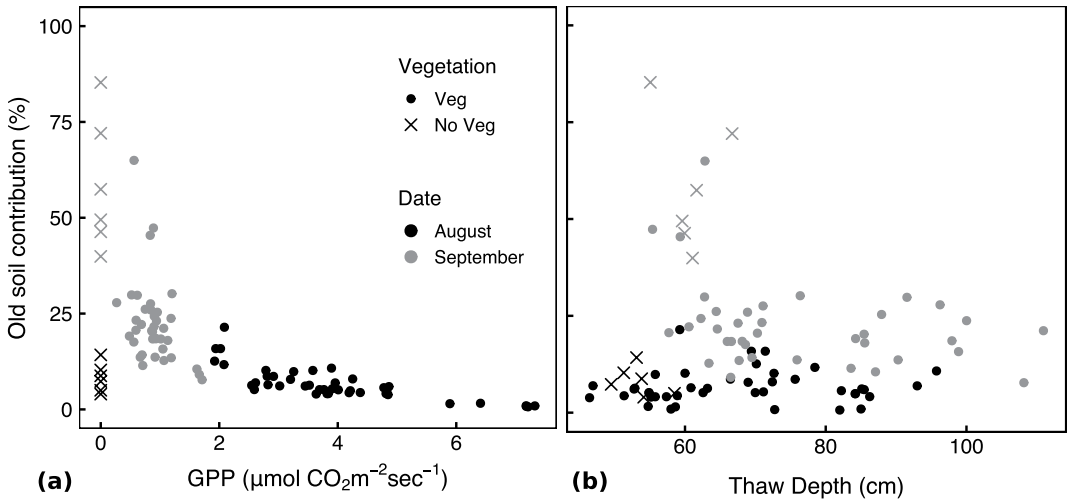

Figure 4. Estimated posterior means of relative old soil contribution to Reco ($P^{\text{Old|Soil}}$, Equation 12) estimated from the partitioning model (Section 2.7.2, Equations 3–13) shown against (a) plot-level GPP and (b) thaw depth (TD). For easier visualization we show only show the posterior means for plot-level $P^{\text{Old|Soil}}$ estimates. There was no systematic bias in the uncertainty (95% CIs) that would change the conclusions based on the patterns observed in the means alone (Figure S5).

increased from August to September across all thaw depths with largest P^{Old} in plots where TD increased to a final depth of between 50 to 60 cm, and plots either had low GPP or no vegetation (Figures 4a and 4b).

4.5. Old Soil Respiration Flux Rates

From August to September flux rates of old soil respiration doubled in vegetated plots and quadrupled in vegetation removal plots (Figure 5a, mean and standard error of old soil flux rates: $\text{Veg}_{\text{August}}$: 0.19 ± 0.013 µmol m^{-2} s^{-1}, No $\text{Veg}_{\text{August}}$: 0.098 ± 0.013 µmol m^{-2} s^{-1}, $\text{Veg}_{\text{September}}$: 0.39 ± 0.027 µmol m^{-2} s^{-1}, No $\text{Veg}_{\text{September}}$: 0.43 ± 0.076 µmol m^{-2} s^{-1}), even as the total Reco flux rates declined by half (Table 1). Mean old soil flux rates were significantly higher in September with no significant difference between vegetation groups (ANOVA of plot-level old soil flux rate: Date $_{\text{F-value}}$: 68.1 ($p < 0.001$, df = 1), Vegetation $_{\text{F-value}}$: 0.290 ($p > 0.05$,

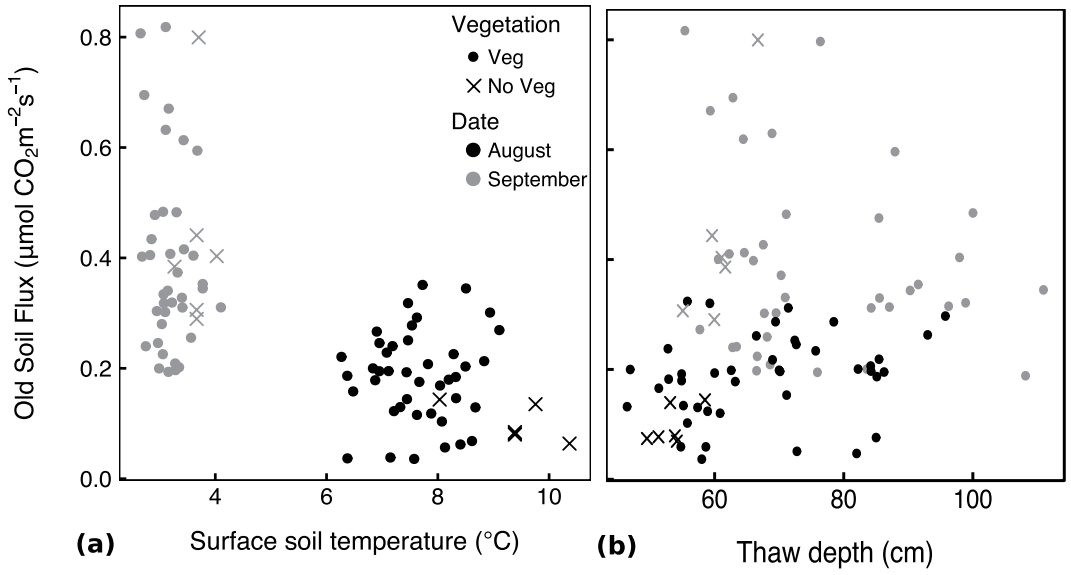

Figure 5. Old soil flux rate of each plot (P^{Old} * Reco µmol m^{-2} s^{-1}) versus (a) surface soil temperature which is the only significant predictor (Table S3) and (b) thaw depth to show patterns.

df = 1), Date * Vegetation $_{\text{F-value}}$: 2.65 ($p > 0.05$, df = 1)). In a regression model with environmental drivers, surface soil temperature was the only significant predictor of old soil respiration rate (Table S3) with higher old soil respiration rates at cooler temperatures (Figure 5a). Despite being nonsignificant, the relationship of old soil flux rates and TD shows highest old soil C fluxes occurred when thaw progressed around TD = 60 cm (Figure 5b), similar to Reco Δ^{14}C (Figure 2b) and P^{Old} (Figure 4b). The soil depths between 40 and 60 cm represent the transition zone between organic and mineral soil horizons and between historic active layer and permafrost zones (see Discussion; Osterkamp et al., 2009; Plaza et al., 2019; Pries et al., 2012).

5. Discussion

Warming and thaw are widely expected to increase soil C loss across northern high latitudes with concomitant increases in plant productivity that could offset soil losses and maintain the C sink capacity of high-latitude ecosystems (McGuire et al., 2018; Meredith et al., 2019; Schuur et al., 2015). In this study, we isolated spatial and temporal variation in thaw depth and plant productivity to examine their effects on Reco Δ^{14}C and estimates of old soil C loss. Overall, plot-level Reco Δ^{14}C signatures were most strongly related to spatial and temporal variation in GPP and surface soil temperature. We were able to account for plant productivity and soil temperature in our process-based partitioning model, and changes in plant productivity therefore do not necessarily obscure old soil C flux estimates. We found that relative old soil contributions to Reco increased from August to September tripling the average old soil C flux despite a seasonal decrease in Reco flux rates and only small additional deepening of thaw. The increase in relative and total old soil C losses was particularly large where seasonal thaw exposed soil layers in the organic to mineral transition horizons (40–60 cm). These results indicate that old soil C losses at the end of the growing season are larger than at near-maximum thaw during the growing season, and that old soil C losses under field conditions may depend less on absolute thaw depth increases and more on soil properties as the soil column thaws.

In the CiPEHR experiment the first three years of warming increased total growing season Reco, driven predominantly by higher autotrophic respiration rates (Hicks Pries et al., 2015, 2016) due to a vigorous growth response by *E. vaginatum* (Salmon et al., 2016). Some studies have suggested that high levels of autotrophic and surface soil respiration can obscure the much lower rates of old soil C respiration when sampling Reco Δ^{14}C of surface fluxes (Nowinski et al., 2010). Our study was designed to examine how old soil C loss estimates would change with differing levels of autotrophic contributions and evaluate old soil C flux rate estimates after an additional 40 cm of thaw at CiPEHR (Mauritz et al., 2017). The Δ^{14}C signature of Reco reflects relative contributions from a mixture of multiple sources and our experimental design specifically sought to maximize relative differences in plant, young soil, and old soil respiration by sampling across a wide range of environmental conditions and plant activity. The combination of vegetation removal, spatial, and seasonal variation in environmental conditions helped interpret Reco Δ^{14}C signatures, and the utility of this design is reflected in the statistical importance of the interaction term between GPP, surface soil temperature, and thaw in the Reco Δ^{14}C regression models that captures these combined conditions (Table 2).

Across a very large range of thaw depths (50–100 cm, Figure 2b), warm surface conditions and high plant productivity were dominant drivers of Reco Δ^{14}C signatures, similar to other permafrost and peatland systems (Hicks Pries et al., 2015; Wilson et al., 2016). During periods of high GPP and warm surface soil conditions (August), Reco Δ^{14}C was most positive with complete vegetation removal (GPP = 0) and in vegetated plots Reco Δ^{14}C decreased as GPP increased. This pattern is consistent with dominant contributions from young surface soil respiration in the absence of plants, resulting in very positive Reco Δ^{14}C (young soil end-member = 71‰, Figure 2c). In vegetated plots Reco Δ^{14}C decreased with increasing GPP which reflects higher autotrophic respiration contributions (plant end-member = 23‰, Figure 2c). The dominance of plant and young soil respiration was expected during the growing season (Hicks Pries et al., 2013, 2016; Schuur et al., 2009) and re-sampling in September revealed that all plots shifted toward older Reco Δ^{14}C with seasonal reductions in GPP, cooling surface soil temperature, and a seasonal thaw extension of ~10 cm across the landscape. Similar seasonal Reco Δ^{14}C declines have been documented in polygonated tundra (Vaughn & Torn, 2018) and at a *Salix*-dominated site in Greenland (Lupascu et al., 2014, 2018), and indicate a landscape-wide shift from plant- and young soil-dominated respiration fluxes to old soil-dominated fluxes after plant senescence and reduced microbial activity in cold surface soil.

The Reco $\Delta^{14}C$ signature depends on relative plant, young, and old soil contributions and thus provides limited insight to the amount of old C respired to the atmosphere. To obtain quantitative estimates of old soil C respiration, the proportional old soil contribution was multiplied by the total Reco flux rate. To our surprise, the proportional increase of old soil C respiration from August to September was so large that despite a decline in total Reco flux, the absolute rate of old soil C respiration increased 2–3-fold. Contrary to our hypothesis that the correlation between old soil C flux and thaw would be stronger following plant senescence, the most deeply thawed plots did not have the largest old soil C flux rates in September. Furthermore, the plot-specific thaw increase from August to September also did not predict old soil C flux rates in September as we might expect if a larger volume of thawed soil organic matter leads to larger old soil C fluxes (results not shown). Instead, the old soil C respiration rates were best predicted by surface soil temperatures, which cooled from August to September across the landscape (Figure 5a). Deep soil layers below 10 cm depth cooled together with the soil surface, though at a slower rate (Table 1, Figure S2), and remained strongly correlated with thaw depth (Figure S1). Thus, deep soil temperatures also do not explain the seasonal increase in old soil C flux.

Examination of the relationship between old soil C flux and thaw depth indicates fluxes of old soil C were highest when thaw extended from 50 to 60 cm (Figure 5b). This suggests a higher potential for old soil C losses at intermediate thaw, relative to deeply thawed plots (>70 cm). High old soil C respiration when intermediate soil depths thawed was also reported from CiPEHR in later sampling years (Pegoraro et al., 2020) and is consistent with estimates of high bulk soil C loss from the organic-to-mineral transition horizon that occurs between 35 and 55 cm (Plaza et al., 2019; Pries et al., 2012).

Taken together, the seasonal increase in old soil respiration with the largest old soil respiration from intermediate thaw depths has two implications. One, that the landscape-scale increase in old soil C fluxes at the end of the growing season depends on surface processes, and two, that upon thawing, the decomposition of soil organic matter varies by soil horizon and does not simply scale with thawed volume of soil. These two results could both be explained by the mechanism of soil priming whereby new inputs of limiting C- and N-substrates can stimulate microbes and promote enhanced soil organic matter decomposition (Kuzyakov, 2010). The correlation between surface soil temperature and old soil C flux can be mechanistically explained by end-of-season increases in plant inputs and reduced activity of surface soil microbes which could increase resource supply to deeper soil horizons and stimulate old soil decomposition (Fontaine et al., 2007). Leaf and root senescence at the end of the growing-season increases C- and N-availability for soil microbes (Cotrufo et al., 2013; Loya et al., 2004; Melillo et al., 1989) and living roots in moist acidic tundra can more than double C-allocation to roots and increase dissolved organic carbon during the autumn senescence period relative to peak growing season (Olsrud & Christensen, 2004, 2011). Declines in surface soil temperature and the onset of freeze-thaw cycles also result in inorganic N flushes from organic tundra soils that exceed N availability during the growing season due to simultaneous reductions in N demand from surface soil microbes and senescing plants (Edwards & Jefferies, 2013; Treat et al., 2016). Lab incubations demonstrate that increased C- and N- inputs stimulate old soil decomposition from mineral and permafrost horizons at our site (Pegoraro et al., 2018) and others across the Artic (Walz et al., 2017; Wild et al., 2014, 2016). These results strongly suggest priming-based increases in old soil C flux driven by the seasonal availability of C- and N- substrates in surface soil layers. In contrast to observations from other peatland sites (Hardie et al., 2009; Walker et al., 2016), we found no significant increase in old soil C flux from vegetated plots compared to non-vegetated plots either during the growing season or after plant senescence. Priming of old soil C decomposition through increased leaching of plant- and soil-derived C- and N-substrate from the surface to deeper in the soil column nonetheless provide a reasonable explanation for the increased old soil C flux reported here and highlights the importance of temporal dynamics for understanding priming effects under field conditions. It is possible that old soil C fluxes would remain high for some time after the end of the growing season. Permafrost soil freezes from the top down and the bottom up, with soil column temperatures remaining warmer than air temperature as water buffers the transition to frozen (Kelley & Weaver, 1969; Zona et al., 2016). At CiPEHR it can take until December or January for soils at 40 cm to freeze (Mauritz et al., 2017). Soil CO_2 losses in winter are a substantial part of the annual ecosystem CO_2 budget in the northern permafrost zone (Natali et al., 2019) and our results suggest that old soil respiration dominates when the growing season ends.

Biogeochemical variation in the soil column can cause substantial differences in permafrost soil decomposition rates (Harden et al., 2012; Hutchings et al., 2019). The elevated old soil C flux detected in plots thawing from 50 to 60 cm may therefore be explained by C- and N- dynamics during thaw of that particular soil horizon. The historic maximum thaw depth (active layer thickness) at this site was around 40–50 cm (Osterkamp et al., 2009) and it is likely that during occasional decadal thaw cycles, soluble organic matter inputs from the active layer became concentrated in this transition zone at the top of the permafrost table (Hutchings et al., 2019; Ping et al., 2015). Lab incubations show that soil from CiPEHR at 45–55 cm is readily decomposable and respires a large fraction of old C (Bracho et al., 2016; Pegoraro et al., 2019). While priming via increased C-inputs may be limited in the transition horizons (Pegoraro et al., 2018; Walz et al., 2017), a flush of inorganic N could stimulate a sizeable increase of soil C decomposition by otherwise extremely N-limited soil micro-organisms (Kuzyakov, 2010; Wild et al., 2018). Notably, the highest potential rates of net N mineralization in soils from CiPEHR have been reported from 55 to 65 cm, with seven times higher net N mineralization compared to shallower soil layers and two to three times higher net N mineralization than deeper layers (Salmon et al., 2018). Alleviation of microbial N limitation may thus explain the high old soil respiration rates when thaw progressed from 50 to 60 cm. It is unclear whether these high old soil C fluxes represent a short-term pulse or a more sustained release of old soil C. If thaw releases a flush of mineralizable N that is then quickly taken up by microbes (Wild et al., 2018), it is possible we missed earlier pulses of elevated old soil respiration from plots that had already thawed beyond 50–60 cm by our first sampling date in August.

Taken together, the seasonal increase in old soil C flux and the high old soil C flux from the organic-to-mineral boundary add evidence that under field conditions old soil decomposition depends in part on substrate and nutrient limitations and is more complex than can be explained by thaw alone (Harden et al., 2012; Koven et al., 2015; Schädel et al., 2016; Treat et al., 2014). Other studies demonstrate that old soil C decomposition also remains limited when thaw is accompanied by water-logging and anoxia (Estop-Aragonés et al., 2018). This is consistent with our results that show no relationship between water table and the amount of old soil C flux. While we did find that Reco $\Delta^{14}C$ signatures were lower when the water table was closer to the surface (significant negative WTD effect in Table 2), the decline in Reco $\Delta^{14}C$ under very wet conditions can be attributed to lower plant and surface soil respiration (Kwon et al., 2019).

One goal of this study was to examine how plant and surface soil respiration impact Reco $\Delta^{14}C$ and consequent estimates of old soil C flux rates. Partitioning based on isotopic variation alone ignores non-isotopic, environmental or biological information that can provide additional constraints on end-member contributions (Ogle et al., 2014). In this study we included plot-level variation in GPP, surface soil temperature, water table depth, and thaw depth in the isotope partitioning model to account for variation of relative old soil contributions to Reco. We also incorporated the fact that plant respiration scales with plant activity by allowing independent GPP measurements to directly constrain plant contributions to Reco, and indirectly constrain soil contributions to Reco (Section 2.7.2, Equations 8–13). Including GPP in the mixing model substantially improved model fit during initial model development and provided more realistic partitioning results. Without GPP constraints, the seasonal decline in Reco $\Delta^{14}C$ from vegetated plots was attributed to increasing plant contributions with estimates of 100% plant contributions in many vegetated plots (results not shown). This occurred because, in vegetated plots, Reco $\Delta^{14}C$ in September came isotopically closer to the plant respiration end-member which lies between surface soil and deep soil end members (Figure 2c). From a process-based understanding, however, we can infer that when plant primary productivity declines, so do plant contributions. Lower Reco $\Delta^{14}C$ from August to September therefore more likely reflect a relative increase in old soil contributions than an increase in plant contributions.

To incorporate seasonal plant activity, we assumed that plant respiration and GPP are linearly related (Section 2.7.1, Equations 3 and 4), which holds true across larger spatial scales (Vicca et al., 2012) and thus seemed appropriate for scaling across plots. The linear assumption has the benefit of simplicity. Nonetheless, we must acknowledge that the assumption of linearity could attenuate end-of-season plant contributions too much. In the tundra, where most vegetation is perennial or evergreen, a nonlinear seasonal function that reflects baseline maintenance respiration might be more accurate. The linear relationship also cannot account for seasonal differences in shoot versus root respiration. For example, if root growth (Blume-Werry et al., 2016) and root C allocation (Olsrud & Christensen, 2011) extend well beyond the

above-ground growing season, a linear relationship would likely under-estimate plant contributions in September. Indeed, in vegetated plots the partitioning model estimated a slight increase in young soil contributions from August to September which could indicate that, for the mixing calculations to produce the correct Reco $\Delta^{14}C$, young soil contributions increased to compensate for too much down-regulation in plant contributions (Figure 3a). Our fundamental knowledge of belowground dynamics (Iversen et al., 2015) and heterotrophic plant tissue respiration is however too limited to adequately represent alternative GPP-Reco dynamics in the partitioning model.

The vegetation removal experiment reduced the end members from three sources (plants, young soil, and old soil) which can be constrained only by statistical portioning, to two sources (young soil, old soil) which can be solved quantitatively with one isotope (Schuur et al., 2003; Trumbore, 2009). Furthermore, the two end-member values for young and old soil in the vegetation removal plots do not overlap and thus provide an unequivocal separation of end member sources. Given the similar CI for plot-level estimates of relative old soil contribution from vegetated and vegetation removal plots (Figure S5) and the tight fit between observed versus predicted Reco $\Delta^{14}C$ ($R^2 = 0.95$, Figure S4), we have high confidence in the model results and that the assumptions we made about GPP constraints on plant contributions did not inflate old soil C loss estimates from vegetated plots in September. We conclude that with the combination of isotopic and non-isotopic constraints it was possible to partition old soil contributions even during periods of high plant activity and surface soil respiration, and that high plant and surface soil respiration did not prevent detection of old soil respiration.

6. Conclusion

A process-based isotopic partitioning approach was crucial for detecting the seasonal increase in old soil C contributions. Isotopic data alone, without the additional biological and environmental constraints, would have incorrectly attributed more negative Reco $\Delta^{14}C$ in September to increasing plant contributions. This highlights the opportunity for greater understanding of permafrost soil processes by combining isotopic and non-isotopic data. Our results demonstrate that old soil C losses do not necessarily increase in direct proportion to deepening thaw and that surface processes dominate spatial variation in old soil C loss. Resampling the same plots in different times of the year revealed that at any given location old soil C losses increase at the end of the growing season, even as total Reco rates decline dramatically. Interestingly, the largest old soil C losses were detected when soil layers at the organic to mineral transition thawed (~50–60 cm, at our site), not from the areas with deepest total thaw. We suggest that both the seasonal increase in old soil C flux and the soil-horizon specific thaw depth can be explained by priming of old soil decomposition via increased N availability. This mechanism should be more directly explored in the future. Regional temperature increases in the fall shoulder season and winter that allow unfrozen soil layers to persist could result in increased N mineralization (Treat et al., 2016) and potentially high loss of older soil C via increasing respiration (Commane et al., 2017; Natali et al., 2019; Zona et al., 2016). Our results support the notion that soil C in the organic-to-mineral or historic active layer-to-permafrost transition zone may be a large source of soil C loss (Plaza et al., 2019). These mid-layers will be the first sections of the profile exposed to warmer temperatures, drainage, and priming via deep root extension or mineralization of in-situ N as the entire Arctic region warms (Hewitt et al., 2019; Keuper et al., 2012; Pegoraro et al., 2018; Salmon et al., 2018; Schuur et al., 2015) and could lead to nonlinearities in projected permafrost climate feedbacks.

Data Availability Statement

All data, as used in this manuscript, are printed in Tables S4–S8 and the complete datasets are archived in the Bonanza Creek LTER Data Catalog (see Table S9). Thanks to Xiaomei Xu at UC Irvine for analysis of $\Delta^{14}C$, to Justin Ledman for constant support in the field, to field technicians who are essential to keeping the CiPEHR experiment running. Thanks to Jessica Guo and Mike Fell for their help with the Bayesian model, and to Jason Downing at Bonanza Creek LTER for tirelessly maintaining our archived data. This project was supported by NSF, DOE, and NPS. All data are archived in the Bonanza Creek LTER Data Catalog and shown in Table S3 and S4.

Acknowledgments
This work was funded by awards to EAG Schuur by U.S. Department of Energy, Office of Biological and Environmental Research, Terrestrial Ecosystem Science (TES) Program, Award #DE-SC0006982 and updated with DE-SC0014085 (2015–2018); National Science Foundation CAREER program, Award #0747195; National Parks Inventory and Monitoring Program; National Science Foundation Bonanza Creek LTER program, Award #1026415; National Science Foundation Office of Polar Programs, Award #1203777.

References

Abbott, B. W., Jones, J., Schuur, E. A. G., Chapin, F. S., Bowden, W. B., Bret-Harte, M. S., et al. (2016). Biomass offsets little or none of permafrost carbon release from soils, streams, and wildfire: An expert assessment. *Environmental Research Letters*, *11*, 034014. https://doi.org/10.1088/1748-9326/11/3/034014

Bauer, J. E., Williams, P. M., & Druffel, E. R. M. (1992). Recovery of submilligram quantities of carbon dioxide from gas streams by molecular sieve for subsequent determination of isotopic carbon-13 and carbon-14 natural abundances. *Analytical Chemistry*, *64*, 824–827. https://doi.org/10.1021/ac00031a024

Blume-Werry, G., Wilson, S. D., Kreyling, J., & Milbau, A. (2016). The hidden season: Growing season is 50% longer below than above ground along an arctic elevation gradient. *New Phytologist*, *209*, 978–986.

Bond-Lamberty, B., Christianson, D. S., Malhotra, A., Pennington, S. C., Sihi, D., AghaKouchak, A., et al. (2020). COSORE: A community database for continuous soil respiration and other soil-atmosphere greenhouse gas flux data. *Global Change Biology*, *26*(12), 7268–7283. https://doi.org/10.1111/gcb.15353

Bracho, R., Natali, S., Pegoraro, E., Crummer, K. G., Schädel, C., Celis, G., et al. (2016). Temperature sensitivity of organic matter decomposition of permafrost-region soils during laboratory incubations. *Soil Biology and Biochemistry*. *97*, 1–14. https://doi.org/10.1016/j.soilbio.2016.02.008

Commane, R., Lindaas, J., Benmergui, J., Luus, K. A., Chang, R. Y. W., Daube, B. C., et al. (2017). Carbon dioxide sources from Alaska driven by increasing early winter respiration from Arctic tundra. *Proceedings of the National Academy of Sciences*, *114*, 5361–5366. https://doi.org/10.1073/pnas.1618567114

Cotrufo, M. F., Wallenstein, M. D., Boot, C. M., Denef, K., & Paul, E. (2013). The microbial efficiency-matrix stabilization (MEMS) framework integrates plant litter decomposition with soil organic matter stabilization: Do labile plant inputs form stable soil organic matter? *Global Change Biology*, *19*, 988–995. https://doi.org/10.1111/gcb.12113

Deane-Coe, K. K., Mauritz, M., Celis, G., Salmon, V., Crummer, K. G., Natali, S. M., & Schuur, E. A. (2015). Experimental warming alters productivity and isotopic signatures of tundra mosses. *Ecosystems*, *18*, 1070–1082. https://doi.org/10.1007/s10021-015-9884-7

DeMarco, J., Mack, M. C., Bret-Harte, M. S., Burton, M., & Shaver, G. R. (2014). Long-term experimental warming and nutrient additions increase productivity in tall deciduous shrub tundra. *Ecosphere*, *5*(6), 1–22. https://doi.org/10.1890/es13-00281.1

Edwards, K. A., & Jefferies, R. L. (2013). Inter-annual and seasonal dynamics of soil microbial biomass and nutrients in wet and dry low-Arctic sedge meadows. *Soil Biology and Biochemistry*. *57*, 83–90. https://doi.org/10.1016/j.soilbio.2012.07.018

Estop-Aragonés, C., Czimczik, C. I., Heffernan, L., Gibson, C., Walker, J. C., Xu, X., & Olefeldt, D. (2018). Respiration of aged soil carbon during fall in permafrost peatlands enhanced by active layer deepening following wildfire but limited following thermokarst. *Environmental Research Letters*, *13*(8), 085002. https://doi.org/10.1088/1748-9326/aad5f0

Fontaine, S., Barot, S., Barre, P., Bdioui, N., Mary, B., & Rumpel, C. (2007). Stability of organic carbon in deep soil layers controlled by fresh carbon supply. *Nature*, *450*, 277–280. https://doi.org/10.1038/nature06275

Gaudinski, J. B., Trumbore, S. E., Davidson, E. A., & Zheng, S. H. (2000). Soil carbon cycling in a temperate forest: Radiocarbon-based estimates of residence times, sequestration rates and partitioning of fluxes. *Biogeochemistry*, *51*, 33–69. https://doi.org/10.1023/a:1006301010014

Gelfand, A. E., & Ghosh, S. K. (1998). Model choice: A minimum posterior predictive loss approach. *Biometrika*, *85*, 1–11. https://doi.org/10.1093/biomet/85.1.1

Gelman, A. (2004). Parameterization and Bayesian Modeling. *Journal of the American Statistical Association*, *99*, 537–545. https://doi.org/10.1198/016214504000000458

Harden, J. W., Koven, C. D., Ping, C.-L., Hugelius, G., McGuire, A. D., Camill, P., et al. (2012). Field information links permafrost carbon to physical vulnerabilities of thawing. *Geophysical Research Letters*, *39*. https://doi.org/10.1029/2012GL051958

Hardie, S. M. L., Garnett, M. H., Fallick, A. E., Ostle, N. J., & Rowland, A. P. (2009). Bomb-^{14}C analysis of ecosystem respiration reveals that peatland vegetation facilitates release of old carbon. *Geoderma*, *153*, 393–401. https://doi.org/10.1016/j.geoderma.2009.09.002

Heffernan, L., Estop-Aragonés, C., Knorr, K.-H., Talbot, J., & Olefeldt, D. (2020). Long-term impacts of permafrost thaw on carbon storage in peatlands: Deep losses offset by surficial accumulation. *Journal of Geophysical Research: Biogeosciences*, *125*, e2019JG005501. https://doi.org/10.1029/2019JG005501

Hewitt, R. E., Taylor, D. L., Genet, H., McGuire, A. D., & Mack, M. C. (2019). Below-ground plant traits influence tundra plant acquisition of newly thawed permafrost nitrogen. *Journal of Ecology*, *107*, 950–962. https://doi.org/10.1111/1365-2745.13062

Hicks Pries, C. E., Logtestijn, R. S. P., Schuur, E. A. G., Natali, S. M., Cornelissen, J. H., Aerts, R., & Dorrepaal, E. (2015). Decadal warming causes a consistent and persistent shift from heterotrophic to autotrophic respiration in contrasting permafrost ecosystems. *Global Change Biology*, *21*, 4508–4519. https://doi.org/10.1111/gcb.13032

Hicks Pries, C. E., Schuur, E. A. G., & Crummer, K. G. (2013). Thawing permafrost increases old soil and autotrophic respiration in tundra: Partitioning ecosystem respiration using δ^{13}C and Δ^{14}C. *Global Change Biology*, *19*, 649–661. https://doi.org/10.1111/gcb.12058

Hicks Pries, C. E., Schuur, E. A. G., Natali, S. M., & Crummer, K. G. (2016). Old soil carbon losses increase with ecosystem respiration in experimentally thawed tundra. *Nature Climate Change*, *6*, 214–218. https://doi.org/10.1038/nclimate2830

Hugelius, G., Strauss, J., Zubrzycki, S., Harden, J. W., Schuur, E. A. G., Ping, C. L., et al. (2014). Estimated stocks of circumpolar permafrost carbon with quantified uncertainty ranges and identified data gaps. *Biogeosciences*, *11*, 6573–6593. https://doi.org/10.5194/bg-11-6573-2014

Hutchings, J. A., Bianchi, T. S., Kaufman, D. S., Kholodov, A. L., Vaughn, D. R., & Schuur, E. A. G. (2019). Millennial-scale carbon accumulation and molecular transformation in a permafrost core from interior Alaska. *Geochimica et Cosmochimica Acta*. *253*, 231–248. https://doi.org/10.1016/j.gca.2019.03.028

Iversen, C. M., Sloan, V. L., Sullivan, P. F., Euskirchen, E. S., McGuire, A. D., Norby, R. J., et al. (2015). The unseen iceberg: Plant roots in arctic tundra. *New Phytologist*, *205*, 34–58. https://doi.org/10.1111/nph.13003

Johansson, M., Terry, T. V. V. C., Bosiö, J., Jackowicz-Korczynski, M., & Christensen, T. R. (2013). Rapid responses of permafrost and vegetation to experimentally increased snow cover in sub-arctic Sweden. *Environmental Research Letters*, *8*, 35025. https://doi.org/10.1088/1748-9326/8/3/035025

Jones, M., Grosse, G., Jones, B. M., & Walter Anthony, K. M. (2012). Peat accumulation in a thermokarst-affected landscape in continuous ice-rich permafrost, Seward Peninsula, Alaska. *Journal of Geophysical Research*, *117*, G00M07. https://doi.org/10.1029/2011jg001766

Kelley, J. J., & Weaver, D. F. (1969). Physical processes at the surface of the Arctic tundra. *Arctic*, *22*, 425–437. https://doi.org/10.14430/arctic3233

Keuper, F., van Bodegom, P. M., Dorrepaal, E., Weedon, J. T., van Hal, J., van Logtestijn, R. S., & Aerts, R. (2012). A frozen feast: Thawing permafrost increases plant-available nitrogen in subarctic peatlands. *Global Change Biology*, *18*, 1998–2007. https://doi.org/10.1111/j.1365-2486.2012.02663.x

Koven, C. D., Lawrence, D. M., & Riley, W. J. (2015). Permafrost carbon-climate feedback is sensitive to deep soil carbon decomposability but not deep soil nitrogen dynamics. *Proceedings of the National Academy of Sciences of the USA*, *112*, 3752–3757. https://doi.org/10.1073/pnas.1415123112

Kuzyakov, Y. (2010). Priming effects: Interactions between living and dead organic matter. *Soil Biology and Biochemistry*, *42*, 1363–1371. https://doi.org/10.1016/j.soilbio.2010.04.003

Kwon, M. J., Natali, S. M., Hicks Pries, C. E., Schuur, E. A., Steinhof, A., Crummer, K. G., et al. (2019). Drainage enhances modern soil carbon contribution but reduces old soil carbon contribution to ecosystem respiration in tundra ecosystems. *Global Change Biology*, *25*, 1315–1325. https://doi.org/10.1111/gcb.14578

Loya, W. M., Johnson, L. C., & Nadelhoffer, K. J. (2004). Seasonal dynamics of leaf- and root-derived C in arctic tundra mesocosms. *Soil Biology and Biochemistry*. *36*, 655–666. https://doi.org/10.1016/j.soilbio.2003.11.009

Lunn, D., Best, N., Spiegelhalter, D., Graham, G., & Neuenschwander, B. (2009). Combining MCMC with "sequential" PKPD modelling. *Journal of Pharmacokinetics and Pharmacodynamics*, *36*, 19. https://doi.org/10.1007/s10928-008-9109-1

Lunn, D. J., Thomas, A., Best, N., & Spiegelhalter, D. (2000). WinBUGS—A Bayesian modelling framework: Concepts, structure, and extensibility. *Statistics and Computing*, *10*, 325–337. https://doi.org/10.1023/A:1008929526011

Lupascu, M., Czimczik, C. I., Welker, M. C., Ziolkowski, L. A., Cooper, E. J., & Welker, J. M. (2018). Winter ecosystem respiration and sources of CO_2 from the high Arctic tundra of Svalbard: Response to a deeper snow experiment. *Journal of Geophysical Research: Biogeosciences*, *123*, 2627–2642. https://doi.org/10.1029/2018JG004396

Lupascu, M., Welker, J. M., Xu, X., & Czimczik, C. I. (2014). Rates and radiocarbon content of summer ecosystem respiration in response to long-term deeper snow in the High Arctic of NW Greenland. *Journal of Geophysical Research: Biogeosciences*, *119*, 1180–1194. https://doi.org/10.1002/2013JG002494

Mauritz, M., Bracho, R., Celis, G., Hutchings, J., Natali, S. M., Pegoraro, E., et al. (2017). Nonlinear CO_2 flux response to 7 years of experimentally induced permafrost thaw. *Global Change Biology*, *23*, 3646–3666. https://doi.org/10.1111/gcb.13661

Mauritz, M., Celis, G., Ebert, C., Hutchings, J., Ledman, J., Natali, S. M., et al. (2018). Using stable carbon isotopes of seasonal ecosystem respiration to determine permafrost carbon loss. *Journal of Geophysical Research : Biogeosciences*, *124*(1), 46–60. https://doi.org/10.1029/2018JG004619

McGuire, A. D., Koven, C., Lawrence, D. M., Clein, J. S., Xia, J., Beer, C., et al. (2016). Variability in the sensitivity among model simulations of permafrost and carbon dynamics in the permafrost region between 1960 and 2009. *Global Biogeochemical Cycles*, *30*, 1015–1037. https://doi.org/10.1002/2016GB005405

McGuire, A. D., Lawrence, D. M., Koven, C., Clein, J. S., Burke, E., Chen, G., et al. (2018). Dependence of the evolution of carbon dynamics in the northern permafrost region on the trajectory of climate change. *Proceedings of the National Academy of Sciences*, *115*, 3882–3887. https://doi.org/10.1073/pnas.1719903115

Melillo, J. M., Aber, J. D., Linkins, A. E., Ricca, A., Fry, B., & Nadelhoffer, K. J. (1989). Carbon and nitrogen dynamics along the decay continuum—Plant litter to soil organic-matter. *Plant and Soil*, *115*, 189–198. https://doi.org/10.1007/bf02202587

Meredith, M., Sommerkorn, M., Cassotta, S., Derksen, C., Ekaykin, A., Hollowed, A., et al. (2019). Chapter 3: Polar regions. In H.-O. Pörtner, D. C. Roberts, V. Masson-Delmotte, et al. (Eds.), *IPCC special Report on the ocean and Cryosphere in a changing climate*.

Natali, S. M., Schuur, E. A. G., Mauritz, M., Schade, J. D., Celis, G., Crummer, K. G., et al. (2015). Permafrost thaw and soil moisture driving CO_2 and CH_4 release from upland tundra. *Journal of Geophysical Research: Biogeosciences*, *120*, 525–537. https://doi.org/10.1002/2014JG002872

Natali, S. M., Schuur, E. A. G., & Rubin, R. L. (2012). Increased plant productivity in Alaskan tundra as a result of experimental warming of soil and permafrost. *Journal of Ecology*, *100*, 488–498. https://doi.org/10.1111/j.1365-2745.2011.01925.x

Natali, S. M., Schuur, E. A. G., Trucco, C., Hicks Pries, C. E., Crummer, K. G., & Baron Lopez, A. F. (2011). Effects of experimental warming of air, soil and permafrost on carbon balance in Alaskan tundra. *Global Change Biology*, *17*, 1394–1407. https://doi.org/10.1111/j.1365-2486.2010.02303.x

Natali, S. M., Watts, J. D., Rogers, B. M., Potter, S., Ludwig, S. M., Selbmann, A. K., et al. (2019). Large loss of CO_2 in winter observed across the northern permafrost region. *Nature Climate Change*, *9*, 852–857. https://doi.org/10.1038/s41558-019-0592-8

Native Land Digital. (2020). Accessed 29 Jul 2020. Retrieved from https://native-land.ca/about/

Nowinski, N. S., Taneva, L., Trumbore, S. E., & Welker, J. M. (2010). Decomposition of old organic matter as a result of deeper active layers in a snow depth manipulation experiment. *Oecologia*, *163*, 785–792. https://doi.org/10.1007/s00442-009-1556-x

Ogle, K., Barber, J., & Sartor, K. (2013). Feedback and Modularization in a Bayesian Meta-analysis of Tree Traits Affecting Forest Dynamics. *Bayesian Anal*, *8*, 133–168. https://doi.org/10.1214/13-BA806

Ogle, K., & Pendall, E. (2015). Isotope partitioning of soil respiration: A Bayesian solution to accommodate multiple sources of variability. *Journal of Geophysical Research: Biogeosciences*, *120*, 221–236. https://doi.org/10.1002/2014JG002794

Ogle, K., Ryan, E., Dijkstra, F. A., & Pendall, E. (2016). Quantifying and reducing uncertainties in estimated soil CO_2 fluxes with hierarchical data-model integration. *Journal of Geophysical Research: Biogeosciences*, *121*, 2935–2948. https://doi.org/10.1002/2016JG003385

Ogle, K., Tucker, C., & Cable, J. M. (2014). Beyond simple linear mixing models: Process-based isotope partitioning of ecological processes. *Ecological Applications*, *24*, 181–195. https://doi.org/10.1890/1051-0761-24.1.181

Olsrud, M., & Christensen, T. R. (2004). Carbon cycling in subarctic tundra; seasonal variation in ecosystem partitioning based on in situ ^{14}C pulse-labelling. *Soil Biology and Biochemistry*, *36*, 245–253. https://doi.org/10.1016/j.soilbio.2003.08.026

Olsrud, M., & Christensen, T. R. (2011). Carbon partitioning in a wet and a semiwet subarctic mire ecosystem based on in situ ^{14}C pulse-labelling. *Soil Biology and Biochemistry 43*, 231–239. https://doi.org/10.1016/j.soilbio.2010.09.034

Osterkamp, T. E., Jorgenson, M. T., Schuur, E. A. G., Shur, Y. L., Kanevskiy, M. Z., Vogel, J. G., & Tumskoy, V. E. (2009). Physical and ecological changes associated with warming permafrost and thermokarst in interior Alaska. *Permafrost and Periglacial Processes*, *20*, 235–256. https://doi.org/10.1002/ppp.656

Pegoraro, E. F., Mauritz, M. E., Ogle, K., Ebert, C. H., & Schuur, E. A. (2020). Lower soil moisture and deep soil temperatures in thermokarst features increase old soil carbon loss after 10 years of experimental permafrost warming. *Global Change Biology*, *27*(6), 1293–1308. https://doi.org/10.1111/gcb.15481

Pegoraro, E., Mauritz, M., Bracho, R., Ebert, C., Dijkstra, P., Hungate, B. A., et al. (2018). Glucose addition increases the magnitude and decreases the age of soil respired carbon in a long-term permafrost incubation study. *Soil Biology and Biochemistry*, *129*, 201–211. https://doi.org/10.1016/j.soilbio.2018.10.009

Pegoraro, E., Mauritz, M., Bracho, R., Ebert, C., Dijkstra, P., Hungate, B. A., et al. (2019). Glucose addition increases the magnitude and decreases the age of soil respired carbon in a long-term permafrost incubation study. *Soil Biology and Biochemistry*, *129*. https://doi.org/10.1016/j.soilbio.2018.10.009

Phillips, C. L., Bond-Lamberty, B., Desai, A. R., Lavoie, M., Risk, D., Tang, J., et al. (2016). The value of soil respiration measurements for interpreting and modeling terrestrial carbon cycling. *Plant and Soil*, *413*, 1–25. https://doi.org/10.1007/s11104-016-3084-x

Ping, C. L., Jastrow, J. D., Jorgenson, M. T., Michaelson, G. J., & Shur, Y. L. (2015). Permafrost soils and carbon cycling. *Soils*, *1*, 147–171. https://doi.org/10.5194/soil-1-147-2015

Plaza, C., Pegoraro, E., Bracho, R., Celis, G., Crummer, K. G., Hutchings, J. A., et al. (2019). Direct observation of permafrost degradation and rapid soil carbon loss in tundra. *Nature Geoscience*, *12*, 627–631. https://doi.org/10.1038/s41561-019-0387-6

Plaza, C., Schuur, E. A. G., & Pegoraro, E. F. (2017). *Eight Mile Lake research watershed, carbon in permafrost experimental heating research (CiPEHR): Physical and chemical properties of soils, 2009–2013*. Bonanza Creek (p. 655). LTER—University Alaska Fairbanks BNZ. https://doi.org/10.6073/pasta/61660d073ee85ed6b0a47b684a919f0e

Pries, C. E. H., Schuur, E. A. G., & Crummer, K. G. (2012). Holocene carbon stocks and carbon accumulation rates altered in soils undergoing permafrost thaw. *Ecosystems*, *15*, 162–173. https://doi.org/10.1007/s10021-011-9500-4

Romanovsky, V. E., Smith, S. L., Isaksen, K., Shiklomanov, N. I., Streletskiy, D. A., Kholodov, A. L., et al. (2017). *Terrestrial permafrost [in Arctic Report card 2017]*.

Salmon, V. G., Schädel, C., Bracho, R., Pegoraro, E., Celis, G., Mauritz, M., et al. (2018). Adding depth to our understanding of nitrogen dynamics in permafrost soils. *Journal of Geophysical Research: Biogeosciences*, *123*, 2497–2512. https://doi.org/10.1029/2018JG004518

Salmon, V. G., Soucy, P., Mauritz, M., Celis, G., Natali, S. M., Mack, M. C., & Schuur, E. A. (2016). Nitrogen availability increases in a tundra ecosystem during five years of experimental permafrost thaw. *Global Change Biology*, *22*, 1927–1941. https://doi.org/10.1111/gcb.13204

Schädel, C., Bader, M. K. F., Schuur, E. A. G., Biasi, C., Bracho, R., Čapek, P., et al. (2016). Potential carbon emissions dominated by carbon dioxide from thawed permafrost soils. *Nature climate change*, *6*, 950–953. https://doi.org/10.1038/nclimate3054

Schädel, C., Koven, C. D., Lawrence, D. M., Celis, G., Garnello, A. J., Hutchings, J., et al. (2018). Divergent patterns of experimental and model-derived permafrost ecosystem carbon dynamics in response to Arctic warming. *Environmental Research Letters*, *13*, 105002. https://doi.org/10.1088/1748-9326/aae0ff

Schädel, C., Schuur, E. A. G., Bracho, R., Elberling, B. O., Knoblauch, C., Lee, H., et al. (2014). Circumpolar assessment of permafrost C quality and its vulnerability over time using long-term incubation data. *Global Change Biology*, *20*, 641–652. https://doi.org/10.1111/gcb.12417

Schuur, E. A. G., Bockheim, J., Canadell, J. G., Euskirchen, E., Field, C. B., Goryachkin, S. V., et al. (2008). Vulnerability of permafrost carbon to climate change: Implications for the global carbon cycle. *BioScience*, *58*, 701–714. https://doi.org/10.1641/b580807

Schuur, E. A. G., Crummer, K. G., Vogel, J. G., & Mack, M. C. (2007). Plant species composition and productivity following permafrost thaw and thermokarst in Alaskan tundra. *Ecosystems*, *10*, 280–292. https://doi.org/10.1007/s10021-007-9024-0

Schuur, E. A. G., Druffel, E. R. M., & Trumbore, S. E. (2016). *Radiocarbon and climate change*. Springer.

Schuur, E. A. G., McGuire, A. D., Romanovsky, V., Schädel, C., & Mack, M. (2018). Chapter 11: Arctic and boreal carbon. In N. Cavallaro, G. Shrestha, R. Birdsey, et al. (Eds.), *Second state of the carbon cycle Report (SOCCR2): A sustained Assessment Report* (pp. 428–468). Washington, DC: U.S. Global Change Research Program.

Schuur, E. A. G., McGuire, A. D., Schädel, C., Grosse, G., Harden, J. W., Hayes, D. J., et al. (2015). Climate change and the permafrost carbon feedback. *Nature*, *520*, 171–179. https://doi.org/10.1038/nature14338

Schuur, E. A. G., & Trumbore, S. E. (2006). Partitioning sources of soil respiration in boreal black spruce forest using radiocarbon. *Global Change Biology*, *12*, 165–176. https://doi.org/10.1111/j.1365-2486.2005.01066.x

Schuur, E. A. G., Trumbore, S. E., Mack, M. C., & Harden, J. W. (2003). Isotopic composition of carbon dioxide from a boreal forest fire: Inferring carbon loss from measurements and modeling. *Global Biogeochemical Cycles*, *17*. https://doi.org/10.1029/2001gb001840

Schuur, E. A. G., Vogel, J. G., Crummer, K. G., Lee, H., Sickman, J. O., & Osterkamp, T. E. (2009). The effect of permafrost thaw on old carbon release and net carbon exchange from tundra. *Nature*, *459*, 556–559. https://doi.org/10.1038/nature08031

Spiegelhalter, D. J., Best, N. G., Carlin, B. P., & Van Der Linde, A. (2002). Bayesian measures of model complexity and fit. *Journal of the Royal Statistical Society: Series B (Statistical Methodology)*, *64*, 583–639. https://doi.org/10.1111/1467-9868.00353

Strauss, J., Schirrmeister, L., Grosse, G., Fortier, D., Hugelius, G., Knoblauch, C., et al. (2017). Deep Yeoman permafrost: A synthesis of depositional characteristics and carbon vulnerability. *Earth-Science Reviews*. *172*, 75–86. https://doi.org/10.1016/j.earscirev.2017.07.007

Sturtz, S., Ligges, U., & Gelman, A. (2005). *R2WinBUGS: A package for Running WinBUGS from R*.

Tanana Chiefs Conference. (2020). Retrieved from https://www.tananachiefs.org/about/communities/

Taylor, M., Schuur, E. A. G., Mauritz, M., Elaine, F. P., Verity, G. S., & Susan, N. (2018). *Eight Mile Lake Research watershed, carbon in permafrost experimental heating and drying research (DryPEHR): Peak growing season aboveground biomass 2011–2017* (p. 502). Bonanza Creek LTER—Univ Alaska Fairbanks BNZ. https://doi.org/10.6073/pasta/3fd711e9c914dd525d698c6e99ddfee5

Treat, C. C., Natali, S. M., Ernakovich, J., Iversen, C. M., Lupascu, M., McGuire, A. D., et al. (2015). A pan-Arctic synthesis of CH_4 and CO_2 production from anoxic soil incubations. *Global Change Biology*, *21*, 2787–2803. https://doi.org/10.1111/gcb.12875

Treat, C. C., Wollheim, W. M., Varner, R. K., & Bowden, W. B. (2016). Longer thaw seasons increase nitrogen availability for leaching during fall in tundra soils. *Environmental Research Letters*, *11*. https://doi.org/10.1088/1748-9326/11/6/064013

Treat, C. C., Wollheim, W. M., Varner, R. K., Grandy, A. S., Talbot, J., & Frolking, S. (2014). Temperature and peat type control CO_2 and CH_4 production in Alaskan permafrost peats. *Global Change Biology*, *20*, 2674–2686. https://doi.org/10.1111/gcb.12572

Trumbore, S. (2000). Age of soil organic matter and soil respiration: Radiocarbon constraints on belowground C dynamics. *Ecological Applications*, *10*, 399–411. https://doi.org/10.1890/1051-0761(2000)010[0399:aosoma]2.0.co;2

Trumbore, S. (2009). Radiocarbon and soil carbon dynamics. *Annual Review of Earth and Planetary Sciences*, *37*, 47–66. https://doi.org/10.1146/annurev.earth.36.031207.124300

Vaughn, L. J. S., & Torn, M. S. (2018). Radiocarbon measurements of ecosystem respiration and soil pore-space CO_2 in Utqiagvik (Barrow), Alaska. *Earth System Science Data*, *10*, 1943–1957. https://doi.org/10.5194/essd-10-1943-2018

Vicca, S., Luyssaert, S., Peñuelas, J., Campioli, M., Chapin, F. S., Ciais, P., et al. (2012). Fertile forests produce biomass more efficiently. *Ecology Letters*, *15*, 520–526. https://doi.org/10.1111/j.1461-0248.2012.01775.x

Vogel, J., Schuur, E. A. G., Trucco, C., & Lee, H. (2009). Response of CO_2 exchange in a tussock tundra ecosystem to permafrost thaw and thermokarst development. *Journal of Geophysical Research*, *114*. https://doi.org/10.1029/2008JG000901

Vogel, J. S., Nelson, D. E., & Southon, J. R. (1987). C-14 background levels in an accelerator mass-spectrometry system. *Radiocarbon*, *29*, 323–333. https://doi.org/10.1017/s0033822200043733

Vonk, J. E., Tank, S. E., Bowden, W. B., Laurion, I., Vincent, W. F., Alekseychik, P., et al. (2015). Reviews and syntheses: Effects of permafrost thaw on Arctic aquatic ecosystems. *Biogeosciences*, *12*, 7129–7167. https://doi.org/10.5194/bg-12-7129-2015

Walker, M. D., Walker, D. A., Welker, J. M., Arft, A. M., Bardsley, T., Brooks, P. D., et al. (1999). Long-term experimental manipulation of winter snow regime and summer temperature in arctic and alpine tundra. *Hydrological Processes*, *13*, 2315–2330. https://doi.org/10.1002/(SICI)1099-1085(199910)13:14/15<2315::AID-HYP888>3.0.CO;2-A

Walker, T. N., Garnett, M. H., Ward, S. E., Oakley, S., Bardgett, R. D., & Ostle, N. J. (2016). Vascular plants promote ancient peatland carbon loss with climate warming. *Global Change Biology*, *22*, 1880–1889. https://doi.org/10.1111/gcb.13213

Walter Anthony, K., Schneider von Deimling, T., Nitze, I., Frolking, S., Emond, A., Daanen, R., et al. (2018). 21st-century modeled permafrost carbon emissions accelerated by abrupt thaw beneath lakes. *Nature Communications*, *9*, 3262. https://doi.org/10.1038/s41467-018-05738-9

Walz, J., Knoblauch, C., Böhme, L., & Pfeiffer, E.-M. (2017). Regulation of soil organic matter decomposition in permafrost-affected Siberian tundra soils—Impact of oxygen availability, freezing and thawing, temperature, and labile organic matter. *Soil Biology and Biochemistry*, *110*, 34–43. https://doi.org/10.1016/j.soilbio.2017.03.001

Wild, B., Alves, R. J. E., Bárta, J., Čapek, P., Gentsch, N., Guggenberger, G., et al. (2018). Amino acid production exceeds plant nitrogen demand in Siberian tundra. *Environmental Research Letters*, *13*, 034002. https://doi.org/10.1088/1748-9326/aaa4fa

Wild, B., Andersson, A., Bröder, L., Vonk, J., Hugelius, G., McClelland, J. W., et al. (2019). Rivers across the Siberian Arctic unearth the patterns of carbon release from thawing permafrost. *Proceedings of the National Academy of Sciences*, *116*, 10280–10285. https://doi.org/10.1073/pnas.1811797116

Wild, B., Gentsch, N., Čapek, P., Diáková, K., Alves, R. J. E., Bárta, J., et al. (2016). Plant-derived compounds stimulate the decomposition of organic matter in arctic permafrost soils. *Scientific Reports*, *6*, 25607. https://doi.org/10.1038/srep25607

Wild, B., Schnecker, J., Alves, R. J. E., Barsukov, P., Bárta, J., Čapek, P., et al. (2014). Input of easily available organic C and N stimulates microbial decomposition of soil organic matter in arctic permafrost soil. *Soil Biology and Biochemistry*, *75*, 143–151. https://doi.org/10.1016/j.soilbio.2014.04.014

Wilson, R. M., Hopple, A. M., Tfaily, M. M., Sebestyen, S. D., Schadt, C. W., Pfeifer-Meister, L., et al. (2016). Stability of peatland carbon to rising temperatures. *Nature Communications*, *7*, 13723. https://doi.org/10.1038/ncomms13723

Zona, D., Gioli, B., Commane, R., Lindaas, J., Wofsy, S. C., Miller, C. E., et al. (2016). Cold season emissions dominate the Arctic tundra methane budget. *Proceedings of the National Academy of Sciences*, *113*, 40–45. https://doi.org/10.1073/pnas.1516017113